Particle production in nucleon induced reactions above 14 MeV with an intranuclear cascade model

H. Duarte

Commissariat à l'Énergie Atomique, DAM/DIF/DPTA/SPN, Boîte Postale 12, F-91680 Bruyères-le-Châtel, France

(Received 11 April 2006; revised manuscript received 21 December 2006; published 22 February 2007)

We present an intranuclear cascade (INC) model which includes the dynamics of the cascade particles and uses in-medium NN elastic cross sections. Our model is still based on the impulse approximation and does not have the complexity of other sophisticated nuclear models. Nevertheless, its results of angle-energy distributions of emitted nucleons in continuum are in good agreement with experimental data for nucleon induced reactions from low intermediate energy to high energy, between 14 MeV and 1.6 GeV, and for light to heavy target nuclei. Comparisons with results of Bertini's INC model and of a previous version of our INC model show the clear contribution of the combined effects of better dynamics and the in-medium NN cross sections. From our results, we conclude that our INC model effectively includes the preequilibrium emission.

DOI: 10.1103/PhysRevC.75.024611 PACS number(s): 24.10.Lx, 25.40.Sc

I. INTRODUCTION

Particle production in nonelastic reactions induced by nucleons has been under investigation for a long time. Serber suggested that nonelastic reactions of intermediate energy hadrons on nuclei may be modeled as a two-step process [1]. He described the first step as a cascade of collisions initiated by the incident particle with the bound nucleons of the target nucleus and propagated by the struck nucleons. In this step, some particles of high energy may be emitted and, at the end, the remaining nucleus can have an excess of internal energy called excitation energy. This is the basis of the intranuclear cascade (INC) model and of the semiclassical preequilibrium model. In the second step, the remaining excited nucleus dissipates its excess of energy by a mechanism that can be viewed as the evaporation of nucleons and light charged particles. The evaporation is in competition with fission for heavy target nuclei and with γ decay. Moreover, evaporation may be replaced by other processes such as fragmentation for light target nuclei or for very high excitation energy.

Even though the INC models [2–11] and some semiclassical preequilibrium models [12–15] may present strong similarities, they differ on physics: the time treatment of the cascade of the binary collisions in the $\{\vec{r}, \vec{p}\}$ phase space requires a Monte Carlo method in the INC model, while in the preequilibrium models, the calculation of particle-hole evolution in energy dimension does not necessarily need stochastic methods even if a Monte Carlo approach of preequilibrium exists [16]. INC and preequilibrium models have also complementary ranges of incident energy. The INC approach takes into account the production of hadrons other than the nucleons (pions and other unstable particles such as Δ resonances) and works well at high energy up to several GeV. The lower energy limit is expected to be around 100–150 MeV [1] above which the impulse approximation is verified. The results of the older INC models are, however, in poor agreement with data at low intermediate energy (below 300 MeV typically) [17–21]. On the contrary, the preequilibrium models deal with nucleon and light nuclei emission below the pion production threshold around 200 MeV.

Despite these discrepancies, the INC and deexcitation models are often used in macroscopic transport codes such as HETC [22], LAHET [23], and MCNPX [24] to generate the products of nonelastic reaction in the intermediate energy range. Indeed, because of the high number of final channels in the particle-nucleus interaction at intermediate and high energy, hadronic cross sections and the differential distribution of particle production are not stored in databases, but rather the Monte Carlo events are calculated on-the-fly by nuclear models. For practical uses such as the simulation of thick target irradiation, such Monte Carlo nuclear models have to combine results of good quality with fast computing time. The lower running energy of the high energy code (stemming from nuclear models) is mainly driven by the upper limit of the evaluated data in low energy macroscopic transport codes like MCNP [25]. Data libraries are generally evaluated below 20 MeV; however, recent studies of accelerator driven systems push this energy limit up to 150 MeV [26], at least for the most important elements.

To improve the results, an additional preequilibrium model is generally included between the INC and deexcitation stages [16,23,24]. On the other hand, other sophisticated nuclear dynamics models such as the Boltzmann-Uehling-Uhlenback (BUU) [27], Boltzmann-Nordheim-Vlasov (BNV) [28], and quantum molecular dynamics (QMD) [29] models have been used for many years to simulate heavy ion reactions above the Fermi energy. They overtook the INC model in the intermediate energy range in heavy ion physics [30] since they deal with the generation and evolution of the mean field in a self-consistent way. Their results are also in good agreement with experimental data in the spallation field (see Refs. [31–33] for the QMD model) at high and low intermediate energy. However, their computing time is very long compared with INC codes, and thus it limits their use in HETC-like codes to simulate nonelastic reactions in macroscopic targets. From this practical point of view, the INC models remain the most

interesting tools for the simulation of high energy nonelastic reactions.

Nevertheless, one may use those sophisticated nuclear models as guidelines and to improve the standard INC approach with some of their physics. We present in this paper the current version of code for our INC model, named BRIC, which is derived from an older version [34] and includes such improvements, the main ones being a better treatment of the dynamics and the in-medium NN cross sections. We use it to simulate nonelastic reactions induced by nucleons on large ranges of incident energies and target nuclei. For instance, we built nuclear databases for soft error studies in microelectronics [35,36], and we have studied specific spallation reactions [37]. Above all, it is important that our INC model provide results in overall good agreement with experimental data and with calculations of preequilibrium models down to at least 100–200 MeV. Another important reason is intrinsic to the INC calculation: low energy intranuclear particles, typically below 100–200 MeV, are statistically present at any time of the INC stage whatever the incident energy. They even often occur at the first collision due to kinematics. By improving reactions at low incident energy, we obtain greater reliability in our data on the emission of low energy nucleons.

This paper is organized as follows. The current version of our INC model is described in Sec. II. After briefly detailing the framework of our calculations and the older version of our code, we compare their respective results for particle production with experimental data in Sec. III. The improvements of the results coming from the combined effects of better dynamics and in-medium NN cross sections are presented and discussed from low intermediate energy to high energy. Then in Sec. IV we suggest some modifications that could improve our model.

II. DESCRIPTION OF OUR INTRANUCLEAR CASCADE MODEL

In our present INC model, incident and outgoing particles are hadrons: nucleons, pions, and Δ resonances, each with their isospin degrees of freedom. They are defined as Dirac functions in phase space $\{\vec{r}_i, \vec{p}_i\}$ with classical trajectories. Their positions and momenta depend on time t and are expressed in the laboratory frame. The series of intranuclear scatterings are limited to the uncorrelated binary collisions. The other processes taken into account are the formation and decay of Δ resonances, and pion production and absorption through the Δ resonance. The range of the incident energy extends up to a few GeV; relativistic kinematics is then used for all incident energies to ensure energy-momentum conservation at the binary collisions.

We will now detail the initialization of the target nucleus and incident hadron and then present the transport algorithm.

A. Initialization in phase space

For a target nucleus of atomic mass A and charge Z, the nucleons are distributed inside a spherical potential. Each of them has a random position, energy-momentum, and isospin according to the matter density distribution, the local momentum distribution, and charge conservation, respectively.

1. Position

At time t_0 the center of mass of the target nucleus is arbitrarily set to $|\vec{r}_G(t_0)| = 0$ in the laboratory frame, where G is the index for the center of mass. The initial position $\vec{r}_i(t_0)$ of nucleon i in the nucleus is randomly sampled from a Woods-Saxon matter density:

$$\rho(r) = \frac{\rho_0(A)}{1 + \exp\frac{r - R_m(A)}{a(A)}}, \tag{1}$$

with the mean radius $R_m(A)$ and the diffuseness $a(A)$ depending on the target mass A.

The parametrizations of a and R_m as functions of the A mass for stable nuclei [38] have been deduced from the adjustment of the Woods-Saxon function on the density matter distributions calculated with the Hartree-Fock-Bogoliubov (HFB) model of Berger *et al.* [39].

$\rho_0(A)$ in Eq. (1) comes from the integration $\int_0^{R_{\text{limit}}} \rho(r) r^2 dr$ where the maximal radius R_{limit} is deduced from the condition

$$\rho(R_{\text{limit}}) = \epsilon_\rho \rho(0), \tag{2}$$

where ϵ_ρ equals 0.005 by default, which corresponds to $R_{\text{limit}} = R_m(A) + 5.29a(A)$.

2. Momentum

The momentum of nucleon i of the target nucleus is randomly sampled in the sphere of radius $p_F(r)$, which is the Fermi momentum at the nucleon position $r = |\vec{r}_i - \vec{r}_G|$:

$$p_F(r) = \sqrt{e_F(r)[e_F(r) + 2m]}, \tag{3}$$

where m is the nucleon mass. The Fermi kinetic energy $e_F(r)$ is deduced from the spherical potential $V(r)$ and the binding energy e_{bind}, such that

$$e_F(r) = -V(r) + e_{\text{bind}} \quad \text{with} \quad e_F(r) \geqslant 0. \tag{4}$$

The constraint $e_F(r) \geqslant 0$ sets the minimal energy to extract a bound nucleon from the nucleus equal to or greater than e_{bind}.

3. Definition of updated nucleus

In our time-dependent approach, global variables describing the system are useful in defining the potential $V(r)$ at time t. The updated nucleus at time t is defined as the sum of all hadrons in the nuclear volume of radius R_{limit} centered at $r_G(t)$. The updated mass and charge numbers come from conservation of the baryon and charge numbers:

$$\begin{aligned} A_{\text{upd}}(t) &= A_{\text{targ}} + \left(1 - \delta_{h_{\text{inc}}\pi}\right) a_{h_{\text{inc}}} - \sum_{j=1}^{n_N(t)} a_j, \\ Z_{\text{upd}}(t) &= Z_{\text{targ}} + z_{h_{\text{inc}}} - \left(\sum_{j=1}^{n_N(t)} z_j + \sum_{k=1}^{n_\pi(t)} z_k \right). \end{aligned} \tag{5}$$

$(A_{\text{targ}}, Z_{\text{targ}})$ and $(a_{h_{\text{inc}}}, z_{h_{\text{inc}}})$ are the mass and charge numbers of the initial target nucleus and of the incident hadron, respectively, and $\delta_{h_{\text{inc}}\pi} = 0$ if the incident hadron h_{inc} is a nucleon, or $\delta_{h_{\text{inc}}\pi} = 1$ if it is a pion. (a_j, z_j) are the mass

and charge numbers of the jth outgoing nucleon, and z_k is the charge of the kth outgoing pion. $n_N(t)$ and $n_\pi(t)$ are the multiplicities of the outgoing nucleons and pions at time t. The mass of the updated nucleus is $M(A_{\rm upd}) = A_{\rm upd}(t)(m - e_{\rm bind})$.

4. Potential

The potential comes from the spatial average of the soft part of the interactions between all hadrons, whereas the collision term simulates the hard core part. We have chosen an energy-independent definition of the potential with spherical symmetry:

$$V(r) = V_N(r) + V_C(r) = V_0 \left(\frac{\rho(r)}{\rho_0(A)} \right)^{2/3} + V_C(r). \qquad (6)$$

V_N and V_C are the nuclear and Coulomb components of the potential, respectively. The $\rho(r)^{2/3}$ dependence of $V_N(r)$ comes from the Fermi gas approximation. In our calculations of nucleon induced reactions, we assume that the density $\rho(r)$ does not change significantly with time, and we use the approximation $\rho(r)(t) = \rho(r)(t_0)$. The amplitude V_0 of $V_N(r)$ is independent of the mass A and is equal to -48 MeV for the baryons (nucleons and Δ's), and to 0 for the pions. The potential of the charged pions is then simply $V_C(r)$.

$V_C(r)$ is the Coulomb field calculated for a uniform sphere of radius R_C and charge $(Z_{\rm upd} - z_{\rm qf})$, where $z_{\rm qf}$ is the charge of the quasifree hadron inside the potential range. R_C is defined by the condition $V(R_C) = e^{(p)}_{\rm bind}$, where $e^{(p)}_{\rm bind}$ is the binding energy of protons. For instance, the Coulomb potential of Δ^{++} compared with the potential of a quasifree proton for the same $Z_{\rm upd}$ is $V_C^{(\Delta^{++})} = 2(Z_{\rm upd} - 2)/(Z_{\rm upd} - 1)V_C^{(p)}$. This $Z_{\rm upd}$ and then the Coulomb potential $V_C(r)$ are updated when a charged hadron goes out. In the present work, we keep the same Coulomb radius R_C when $Z_{\rm upd}$ or $A_{\rm upd}$ change. The Coulomb barrier of a charged baryon is defined by the condition $V(r) > 0$.

5. Incident hadron

At time t_0, the position $\vec{r}_{\rm inc}$ of the incident hadron is initialized at a random impact parameter $b_{\rm inc}$ and a random polar angle at the surface of the nucleus ($r_{\rm inc} = R_{\rm limit}$) with the condition $\vec{r}_{\rm inc} \cdot \vec{p}_{\rm inc} < 0$. The starting time of a reaction, t_0, is arbitrarily fixed to 0 fm/c. The kinetic energy of an incident nucleon is simply increased by $V(R_{\rm limit})$ to calculate the energy balance at the end of the INC stage, and the momentum $|\vec{p}_{\rm inc}|$ is scaled accordingly to keep energy-momentum conservation.

B. Transport algorithm

1. Bound (spectator) nucleons and quasifree hadrons

Two classes of particles are defined in our approach: the bound nucleons and all the other particles. The nucleons that have a kinetic energy lower than their potential value $V_N(r)$ are bound nucleons and stay static in phase space. The other particles, particularly nucleons with kinetic energy higher than $V_N(r)$, move in the potential according to equations of motion detailed below. They are called quasifree because they have enough energy to exit the nuclear volume (a positive charged particle can cross the Coulomb barrier by tunneling according to a transmission coefficient, as will be shown later). If they leave the nucleus, they become outgoing particles. The Δ's and pions are regarded as quasifree particles whatever their kinetic energy since they can interact inelastically with a nucleon. The state of a nucleon, bound or quasifree, changes only when it collides with another hadron. At time $t_0 = 0$, the incident hadron is the only quasifree particle.

2. Equations of motion

The position and momentum of a quasifree hadron between two processes (collision, resonance decay, or reflexion at nucleus surface) are given classically by the following equations of motion (we assume $c = 1$):

$$\frac{d\vec{p}_i}{dt} = -\vec{\nabla}_{r_i} V(|\vec{r}_i - \vec{r}_G|), \qquad (7)$$

$$\frac{d\vec{r}_i}{dt} = \frac{\vec{p}_i}{E_i}, \qquad (8)$$

where the total energy of the hadron E_i is used to take account of the relativistic kinematics.

This kind of equation of motion is intrinsically treated in sophisticated dynamics models such as the BUU model [27] or others (e.g., BNV [28]) and may be even found in the INC model [40]. We point out now the main differences between our approach and these models:

(i) Only the quasifree hadrons obey these equations in phase space.
(ii) Hadrons are Dirac functions in phase space, so we do not use the N-test-particle method proposed by Wong [41] and used in the BUU model [42].
(iii) The potential V is not calculated self-consistently during the cascade stage, but it is the parametrization (6).

The two first points are required to minimize computing time; furthermore, we do not expect a large evolution of the bound nucleons distribution before the end of the INC stage in hadron induced reactions. For the third point, the deformation of the shape of $V(r)$ in Eq. (6) can be assumed to also be small in hadron induced reaction. But above all, the single-particle approach implicitly used in INC models is not adapted to computing the density and potential self-consistently.

The trajectory of a quasifree hadron in the position space is curvilinear between two time steps t_n and t_{n+1}, that is,

$$\vec{r}_i(t_{n+1}) = \vec{r}_i(t_n) + \frac{\vec{p}_i(t_n)}{E_i(t_n)}\Delta t - \frac{(\vec{\nabla}_{r_i} V)(t_n)}{E_i(t_n)} \frac{(\Delta t)^2}{2}, \qquad (9)$$

and its momentum changes accordingly to

$$\vec{p}_i(t_{n+1}) = \vec{p}_i(t_n) - \left(\vec{\nabla}_{r_i} V \right)(t_n)\Delta t.$$

The total energy of the quasifree hadron is updated assuming it is on the mass-shell.

The momentum and position of the nucleus center of mass are then calculated as

$$\vec{p}_G(t_{n+1}) = \vec{p}_G(t_n) + \sum_{k\ \text{quasifree}} \left(\vec{\nabla}_{r_k} V\right)(t_n)\Delta t,$$

$$\vec{r}_G(t_{n+1}) = \vec{r}_G(t_n) + \frac{\vec{p}_G(t_{n+1}) + \vec{p}_G(t_n)}{2M(A_{\text{upd}})}\Delta t.$$

The drift of the c.m. position $\vec{r}_G$ is, of course, higher for light target nuclei than for medium and heavy nuclei.

The time step Δt is by default 1 fm/c if no process occurs for the quasifree hadron, or it is the time interval to its next process, then in this case it is less than 1 fm/c. We checked that the results are statistically the same for lower default values of Δt and for 1 fm/c. The conservation of global energy is required at each time step to obtain a good energy balance at the end of the INC stage.

3. *Reflexion at the surface of the nucleus*

The refraction of quasifree hadrons inside the potential is implicitly dealt with by the equations of motion. However, the quantum reflexion of a particle on the potential well has to be added for both neutral and charged particles.

For each particle that would reach the edge of the nucleus at R_{limit}, we compute a transmission factor T_{WKB} in the WKB approximation [43] with the potential $V(r)$ [Eq. (6)]. Although it is not symmetric, the potential is sufficiently smoothed to assume that the final transmission factor below, near, and above the top of the potential is close to $T = T_{\text{WKB}}/[1 + T_{\text{WKB}}]$ [44].

This transmission factor T is applied to the candidate outgoing particle. If the candidate particle is not allowed to leave out the nuclear volume, its momentum is reflected inside the nucleus at the surface according to the optical law: the longitudinal momentum along the axis joining the center of nucleus to the point of reflexion is reversed after reflexion.

C. Collision term

The positions of binary collisions are calculated in space with the algorithm of the distance of closest approach: a collision occurs if

$$d_{ij}(t_{\text{min}}) = |\vec{r}_i(t_{\text{min}}) - \vec{r}_j(t_{\text{min}})| < \sqrt{\sigma_{\text{tot}}/\pi},$$

where $r_i(t)$ is given by Eq. (9), t_{min} is the time of closest approach (d_{ij} is minimal at $t = t_{\text{min}}$), and σ_{tot} is the total cross section of the ij pair. This method is often used to simulate the hard core part of the hadron-hadron interaction when hadrons are described as points in phase space, as in INC and BUU models [9,40,42,45], or as Gaussians in phase space, as in QMD models [29].

In our calculation, the distance of closest approach $d_{ij}(t_{\text{min}})$ is defined in the laboratory frame and not in the center of mass of the two colliding particles as in the model of Cugnon [46] and Wolf *et al.* [45]. The covariant calculation proposed by Kodama *et al.* [47] is not used here because most of the collisions occur between a quasifree hadron and a spectator nucleon. Their impact parameter b depends on the initial positions of the spectator nucleons and then on the local density. In the nucleus rest frame, the ordering of these collisions with a bound nucleon is straightforward. The problem of collision ordering in a no-covariant calculation should be more important for the scattering of two quasifree hadrons. Since the number of such scatterings are less significant in hadron induced reactions than in heavy ion physics, we stay in the laboratory frame to order the scatterings.

The following hadronics reactions are treated explicitly:

(i) $NN \to NN$ (elastic scattering)
(ii) $\Delta\Delta \to \Delta\Delta$ (elastic scattering)
(iii) $NN \rightleftharpoons N\Delta$
(iv) $N\pi \rightleftharpoons \Delta$.

Other reactions in which the N^* resonance appears, such as $\Delta\pi \rightleftharpoons N^*$ and the double pion production, are not included. From the physics point of view, the upper limit of the incident energy is then around 1.5 GeV for the nucleon induced reaction and around 300 MeV for the pion induced reaction; our code of the INC model can nevertheless compute above these limits up to 10–15 GeV. The pion-pion elastic scattering is not dealt with in the present model.

All differential and integrated cross sections discussed here depend on the isospins of initial and final hadrons.

1. *NN elastic cross section*

We adopt in-medium cross sections for the nucleon-nucleon elastic channel. Indeed, they differ noticeably from the free cross sections at low c.m. energy. However, we have the choice of several calculations of in-medium cross sections. Some depend on the density [48], others on the temperature [49].

The density-dependent in-medium cross sections of Li and Machleidt [48] have already been used with the INC model of Bertini [50]. The authors of Ref. [50] reported that using the in-medium cross sections improves the angular spectra of produced neutrons in comparison with calculations with the free cross sections. Moreover, the parametrizations of Li and Machleidt are well adapted to our approach, because the matter density is well defined at any point of the nucleus in our model. For these two reasons, we have chosen their parametrization that we recall below.

The elastic cross sections $\sigma_{\text{el}\,(pn)}$ $\sigma_{\text{el}\,(pp)}$ are the free ones $\sigma^{(\text{free})}_{\text{el}\,(pn)}$ and $\sigma^{(\text{free})}_{\text{el}\,(pp)}$ scaled by factors f_{pn} and f_{pp}, respectively, that depend on the kinetic energy e_{lab} of the incident nucleon in the rest frame of the target nucleon and on the local density ρ [48]:

$$f_{pn}(e_{\text{lab}}, \rho) = \frac{1 + 0.0034\, e_{\text{lab}}^{1.51}\rho^2}{1 + 21.55\,\rho^{1.34}}, \tag{10}$$

$$f_{pp}(e_{\text{lab}}, \rho) = \frac{1 + 0.1667\, e_{\text{lab}}^{1.05}\rho^3}{1 + 9.704\,\rho^{1.2}}. \tag{11}$$

The free elastic $\sigma^{(\text{free})}_{\text{el}\,(pn)}$ and $\sigma^{(\text{free})}_{\text{el}\,(pp)}$ and total cross sections are parametric functions of the c.m. energy $\sqrt{s} = \sqrt{2m(e_{\text{lab}} + 2m)}$ of the two colliding nucleons that we have fitted on experimental data.

To perform calculations above 800 MeV/c ($e_{\rm lab} >$ 300 MeV), we assume a linear interpolation of the density-dependent factors from 800 to 1100 MeV/c:

$$f'(p_{\rm lab},\rho) = \begin{cases} f & p_{\rm lab} \leqslant 800\,{\rm MeV}/c \\ f + (1-f)\dfrac{p_{\rm lab}-800}{1100-800} & 800 < p_{\rm lab} \leqslant 1100\,{\rm MeV}/c \\ 1 & 1100 < p_{\rm lab}. \end{cases} \tag{12}$$

The energy intervals of this interpolation have been chosen to connect smoothly our parametrization of the elastic cross sections fitted on experimental data and the in-medium elastic cross sections of Li and Machleidt.

2. Differential NN elastic cross sections

The differential cross sections of elastic scattering in the NN c.m. frame are parametric functions of the relativistic invariant $\tilde{t} = 2p^2_{\rm c.m.}(1-\cos\theta_{\rm c.m.})$ fitted on experimental data of the free processes. The pp and nn elastic differential cross section is parametrized with

$$\frac{d\sigma_{pp}}{d\Omega} = \frac{\sigma^{\rm (free)}_{{\rm el}\,(pp)}(s)}{\mathcal{N}_{pp}}\left(e^{B_{pp}\tilde{t}} + a_{pp}\cdot e^{B'_{pp}\tilde{t}}\right), \tag{13}$$

where $\mathcal{N}_{pp}$ is a normalization factor, $\mathcal{N}_{pp} = 2\int(e^{B_{pp}\tilde{t}} + a_{pp}\cdot e^{B'_{pp}\tilde{t}})d\Omega$. The fit of the parametric function (13) on experimental data gave a sets of values for the parameters a_{pp}, B_{pp}, B'_{pp}. Each set of values was then fitted to give the energy-dependent parametrizations, where $e_{\rm lab}$ is in MeV,

$$B_{pp}(s) = \begin{cases} 0 & e_{\rm lab} \leqslant 300 \\ 9.87\times10^{-8}\,(e_{\rm lab}-300)^3 & 300 < e_{\rm lab} \leqslant 670 \\ 4.56\times10^{-3}\,(e_{\rm lab}-670)+4.76 & 670 < e_{\rm lab} \leqslant 1100 \\ 7.4\left(1+\frac{3\times10^5}{(e_{\rm lab}-300)^{2.23}}\right)^{-1} & 1100 < e_{\rm lab}, \end{cases}$$

$$a_{pp}(s) = \begin{cases} 0.2 & e_{\rm lab} \leqslant 670 \\ 97.02\times10^3\exp\left(-2\times10^{-2}\,e_{\rm lab}\right)+0.053 & 670 < e_{\rm lab} \leqslant 1100 \\ 0.28\exp\left(-1.5\times10^{-3}\,e_{\rm lab}\right) & 1100 < e_{\rm lab}, \end{cases} \tag{14}$$

$$B'_{pp}(s) = \begin{cases} 0 & e_{\rm lab} \leqslant 670 \\ \left(\frac{e_{\rm lab}-670}{217.49}\right)^3\exp\left(-\frac{e_{\rm lab}-670}{200}\right) & 670 < e_{\rm lab} \leqslant 1100 \\ 1.94\exp\left(-7\times10^{-4}\,e_{\rm lab}\right) & 1100 < e_{\rm lab}. \end{cases}$$

The parametrization of the np elastic differential cross section is detailed in Ref. [34].

3. $N\Delta$ cross sections

We deduce the inelastic cross sections $\sigma(NN\to N\Delta)$ from $\sigma^{\rm (free)}_{{\rm tot}\,(NN)} - \sigma^{\rm (free)}_{{\rm el}\,(NN)}$, each channel with its isospin factor [45,51]. In this inelastic NN collision, the mass of the Δ is randomly sampled from the momentum-dependent Breit-Wigner distribution [52], that is,

$$f(M) = \frac{4M_0^2\Gamma^2(M)}{\left(M^2-M_0^2\right)^2 + 4M_0^2\Gamma^2(M)}, \tag{15}$$

with

$$\Gamma = \left(\frac{q}{q_r}\right)^3\frac{M_0}{M}\left(\frac{v(q)}{v(q_r)}\right)^2\Gamma_r, \tag{16}$$

where q is the c.m. momentum in the πN channel. The index r refers to the values calculated at mass $M_0 = 1232$ MeV, $\Gamma_r = 110$ MeV, and

$$v(q) = \frac{\beta_r^2}{\beta_r^2+q^2}, \tag{17}$$

with $\beta_r = 300$ MeV.

The parametric function of $d\sigma/d\Omega(NN\to N'\Delta)$, the distribution of N' angle in the c.m. frame of the colliding nucleons, is the one proposed by Cugnon *et al.* for np inelastic collision [53] and a polynomial function for pp and nn inelastic collisions. Rupp and collaborators [54] showed indeed that the double differential cross section $d^2\sigma/d\Omega dM_{\pi^+p}$ depends on the invariant mass $M(\pi^+p)$ in the $pp\to\pi^+pn$ reaction at 800 MeV. They fitted the distribution

$$A + B\cos^2\theta + C\cos^4\theta \tag{18}$$

on their data and obtained a C/A ratio consistent with zero and a B/A ratio decreasing when the $M(\pi^+p)$ mass increases. We follow the same prescription for the $pp\to\Delta^{++}n$, $pp\to\Delta^+p$ reactions and the isospin corresponding nn reactions. We

assume that there is only an S state in the low c.m. momentum of Δ, and that the B/A and C/A parametric functions are

$$\frac{B}{A}(M_\Delta) = \frac{7}{1+\exp\left(\frac{M_\Delta-1200}{25}\right)}, \tag{19}$$

$$\frac{C}{A}(M_\Delta) = \frac{4}{1+\exp\left(\frac{M_\Delta-1100}{20}\right)}, \tag{20}$$

where M_Δ is the mass of the Δ resonance that was sampled from Eq. (15).

The Δ resonance either decays into pion and nucleon or is absorbed in a $N\Delta \to NN$ collision. The decay process proceeds after a time t_{decay} sampled according to its lifetime $\frac{E_\Delta}{M_\Delta}\frac{\hbar}{\Gamma}$ in the nucleus frame with Γ defined by Eq. (16) if no $N\Delta$ collision happens before t_{decay}. A pion-nucleon P-wave state is assumed after the decay and takes into account isospin conservation. For the resonance absorption, the cross section is calculated with the detailed balance principle [45,55]. Pion absorption occurs when the distance of minimal approach $d_{N\text{pion}}$ verifies the condition $d_{N\text{pion}} < \sqrt{\sigma(N\text{pion})/\pi}$, $\sigma(N\text{pion})$ being the free cross section. The produced Δ resonance in pion absorption has a lifetime inversely proportional to Eq. (16).

For the scarce $\Delta\Delta$ collisions, we use $\sigma'_{\Delta\Delta}(\sqrt{s}) = \sigma'_{NN}(\sqrt{s})$, where σ' stands for the elastic cross section σ_{el}, and the differential elastic cross section $d\sigma_{\text{el}}/d\Omega$. We do not take into account the inelastic $\Delta\Delta$ channels since no other hadronic resonance is taken into account in our present model.

Final state of the hadron-hadron scattering in nuclear medium is completely defined after the application of Pauli blocking.

4. Pauli blocking

In the cascade model of Cugnon and the dynamic models of heavy ion inelastic reaction such as BUU or QMD, Pauli blocking is based on the occupation rate in phase space. This method simulates efficiently the Pauli exclusion principle but is more adapted for the N-test-particle approach [42] than for single-particle models like INC. In our model, the assumption that the bound nucleons stay static in phase space produces a default with such a definition of Pauli blocking: a fraction of the events have a negative excitation energy (the excitation energy is deduced from conservation laws as it will be shown in Sec. II D); moreover, the fraction of such events increases when the incident energy decreases. For instance, around 2% of events have on average -10 MeV of excitation energy for a 1 GeV proton incident on lead (we have seen negative values down to -75 MeV). This is the result of the energy transfer from the nucleus to the incident hadron that escapes the nucleus (the bound nucleon after NN collision has a lower energy than before the collision). If such an energy transfer may be expected some time after the beginning of the cascade when some holes were created in the nuclear medium, it should be forbidden for the incident hadron since it must see an unperturbed nucleus with an entire occupation of the levels below the Fermi energy.

Since the default with the occupation rate definition grows when the incident energy decreases, the Pauli blocking is implemented in what we call the sharp cutoff definition which is generally used in other cascade models [2,4,6,7]: the momentum p_{after} of the nucleon after collision is compared with the local Fermi momentum p_F at position r of the nucleon according to

$$f_{\text{sharp}}(p_{\text{after}}, r) = \theta(p_{\text{after}} - p_F(r)), \tag{21}$$

where θ is the Heaviside function. The collision process with one (or two) nucleon in final state is not allowed if the factor $1 - f_{\text{sharp}}$ equals 0 for at least one final nucleon.

It is interesting to notice that the difference of the excitation energy at the end of the cascade for the two definitions of Pauli blocking (occupation rate or sharp cutoff) is not negligible. For instance, the mean excitation energy in the 800 MeV proton induced reaction on lead is about 109 MeV with the occupation rate definition and 154 MeV with the sharp cutoff definition. That corresponds to a difference of around 5 neutrons for the mean multiplicity of evaporated neutrons, since the latter depends greatly on the excitation energy at the end of the cascade stage.

Though a more accurate Pauli blocking should stand between these two definitions, the sharp cutoff Pauli blocking is used by default in our calculations.

5. Q value

In a quasielastic nucleon-nucleus reaction, the upper limit of the spectra of produced nucleons depend on the Q value of the reaction $X(N, N')$. Most INC models overestimate the upper limit of the differential cross sections $d\sigma/dE_n$ of the (p, xn) reaction when $|Q(p, n)|$ is large (see, for instance, Refs. [56,57]). This discrepancy may occur also in the (n, xp) reaction. The main reason for this artifact comes from the use of the same binding energy e_{bind} for protons and neutrons of the target nucleus.

To improve the upper limit part of the spectra, we take into account the Q value in the first effective $N_{\text{inc}}N_{\text{bound}}$ elastic collision of the reaction induced by the incident nucleon N_{inc}. An effective collision means that it is allowed by the Pauli exclusion principle. The Q value is taken into account for any nucleon induced reaction. No correction has been included for pion induced reactions at this moment.

D. Conservation laws and end of the INC stage

Similar to the way we defined the updated mass A_{upd} and charge Z_{upd} (Sec. II A3), the excitation energy U_{exc} of the system may be defined at time t by

$$U_{\text{exc}}(t) = e_{\text{inc}} + \delta_{h_{\text{inc}}\pi} m_\pi + \left(1 - \delta_{h_{\text{inc}}\pi}\right) e_{\text{bind}} - \left(\sum_{j=1}^{n_N(t)} (e_j + e_{\text{bind}}) + \sum_{k=1}^{n_\pi(t)} (e_k + m_\pi) \right) - E_{\text{rec}}, \tag{22}$$

where e_{inc} is the kinetic energies of the incident hadron of type h_{inc}, and e_j and e_k the kinetic energies of the jth outgoing hadron and the kth outgoing pion, respectively. m_π is the pion

mass. The recoil energy $E_{\rm rec}$ of the updated nucleus is deduced from momentum conservation as

$$E_{\rm rec} = \frac{P_{\rm rec}^2}{2\mathcal{M}(A_{\rm upd})}, \quad \text{with} \quad \vec{P}_{\rm rec} = \vec{p}_{\rm inc} - \sum_{l=1}^{n_N+n_\pi} \vec{p}_l,$$

since the target nucleus has no momentum at time $t_0 = 0$.

1. Excitation energy of bound nucleons

The expression $U_{\rm exc}(t)$ [Eq. (22)] has to be interpreted as the excess energy of the overall nucleus $[A_{\rm upd}(t), Z_{\rm upd}(t)]$ compared to its rest mass. From now on, it is called the total excitation energy since it is measured from the outside of the system at time t. In this definition, there is no difference between the quasifree hadrons and the bound nucleons in the potential well. As a consequence, $U_{\rm exc}(t)$ starts at a high value, the incident energy $e_{\rm inc}$ (plus the mass of pion in case of pion induced reaction), and decreases with time. The solid lines in Fig. 1 show the mean values of the total excitation energy distribution as a function of time $\langle U_{\rm exc}\rangle(t)$ for six proton induced reactions on ^{208}Pb. At early time, the nuclear volume contains not only the bound nucleons but also the fast quasifree hadrons. As the latter escape the volume, the mean excitation energy decreases rapidly to reach an asymptotic value. In the case of the 800 MeV proton on ^{208}Pb, the mean energy $\langle U_{\rm exc}\rangle(t)$ converges to 154 MeV after 80 fm/c. For the 45 MeV reaction, a compound nucleus is formed with $\langle U_{\rm exc}\rangle(t) \sim 40$ MeV before 100 fm/c. This indicates that at these low incident energies, a large part of incident protons are captured by the target nucleus in the INC step.

However, the fact that $U_{\rm exc}(t)$ starts with a high mean value at $t_0 = 0$ fm/c is rather an unpleasant property. Indeed, one may expect that the nucleus at the start of the cascade is not excited with all the incident energy but gets small quantities of energy at each intranuclear collision. The hadrons which are largely above the Fermi energy should not be included in the excited nucleus definition, since they have enough energy to go out of the nuclear volume at any time and they can leave it if no process prevents them. Equation (22) should only be considered at the end of the cascade stage instead of at any time t.

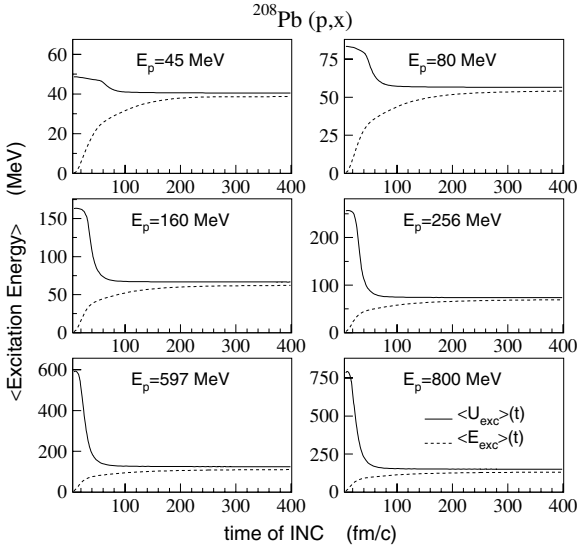

FIG. 1. Time-dependent mean excitation energies $\langle U_{\rm exc}\rangle$ and $\langle E_{\rm exc}\rangle$ defined by Eqs. (22) and (23), respectively, for proton induced reactions on ^{208}Pb at six incident energies.

This suggests that we define a preresidual nucleus composed of bound nucleons only. The preresidual nucleus is different from the updated nucleus $(A_{\rm upd}, Z_{\rm upd})$ since the updated nucleus includes the bound nucleons and the quasifree hadrons that are inside the nuclear volume. Then, the excitation energy of the preresidual nucleus has to converge to $U_{\rm exc}(t_{\rm cut})$ event by event where $t_{\rm cut}$ is the time that stops the cascade stage as we discuss in the next section.

We define the excitation energy of the preresidual nucleus as the sum of the energy losses of the quasifree particles in the bound system at each collision:

$$\begin{aligned} E_{\rm exc}(t) &= \sum_{b,t>t_b} (e_F(r_b) - e_b^<(t_b)) + \sum_{c,t>t_c} (e_c^>(t_c) - e_F(r_c)) \\ &= \sum_{b,t>t_b} \delta e_{b\to {\rm qf}}(t_b) + \sum_{c,t>t_c} \delta e_{{\rm qf}\to c}(t_c). \end{aligned} \tag{23}$$

Here, $e_b^<(t_b)$ is the kinetic energy of the bound nucleon b before its effective collision at time t_b with a quasifree particle, and $e_c^>(t_c)$ is the kinetic energy of the nucleon c that is captured (or becomes bound) after its effective collision at time t_c. And $e_F(r_i)$ is the local Fermi energy at position r_i of nucleon i.

Then, $\delta e_{b\to {\rm qf}}(t_b) = (e_F(r_b) - e_b^<(t_b))$ is the amount of energy needed to extract the bound nucleon from the Fermi sea when the *bound* $\to$ *quasifree* transition occurs in a collision, while $\delta e_{{\rm qf}\to c}(t_c) = (e_c^>(t_c) - e_F(r_c))$ is the energy left in the preresidual nucleus in a *quasifree* $\to$ *captured* transition.

The *bound* $\to$ *captured* transition occurs in an effective collision induced by a quasifree hadron when the bound nucleon goes in the gap between the Fermi energy and the top of the potential well $V_N(r)$. The energy left in the preresidual nucleus is then calculated with these time and position conditions ($r_c = r_b; t_c = t_b$), giving $\delta e_{b\to c}(t_b) = (e_F(r_b) - e_b^<(t_b)) + (e_c^>(t_c) - e_F(r_c)) = (e_c^>(t_b) - e_b^<(t_b))$. This energy deposition is implicitly included in (23) when the *bound*$\to$*captured* transition occurs.

The hashed lines of Fig. 1 are the mean excitation energy $\langle E_{\rm exc}\rangle$ of the preresidual nucleus as a function of time for the proton on lead reaction at six incident energies. With the approach based on the freezing of spectator (bound) nucleons and the sharp cutoff Pauli blocking, it is an increasing function of time with an asymptotic value. One may notice that this asymptotic value is lower than that of $\langle U_{\rm exc}\rangle$. This difference has two causes: first, some quasifree hadrons are still in the nuclear volume at time t, then a part of the kinetic energy of the quasifree nucleons and the mass excess of Δ's and pions inside the nucleus is included in the $U_{\rm exc}(t)$ expression, while it is not taken into account in $E_{\rm exc}(t)$; second, the recoil and binding energies are absent in the calculation of $E_{\rm exc}(t)$. The two excitation energies agree event by event when these two missing terms are taken into account.

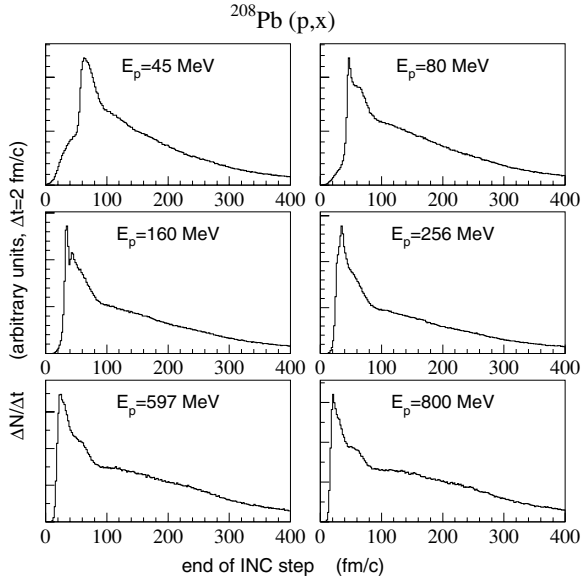

FIG. 2. Distribution of the end of INC step for proton induced reactions on ^{208}Pb at six incident energies. Ordinate is number of events in arbitrary units. The end of INC step is determined when no more quasifree hadrons are inside the nuclear volume of radius R_{limit}. Events with at least one quasifree hadron inside the nucleus after 400 fm/c are not shown here.

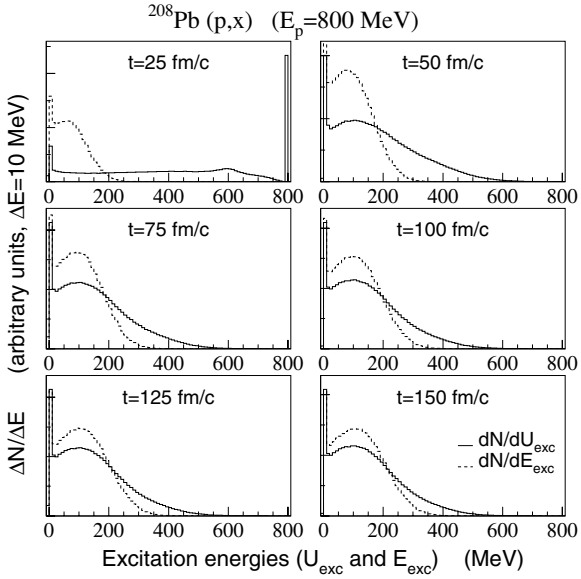

FIG. 3. Distribution of excitation energies U_{exc} and E_{exc} defined by Eqs. (22) and (23), respectively, at six different times for the 800 MeV proton induced reaction on ^{208}Pb.

2. End of the INC stage

One important question is at which time limit should the cascade stage be stopped? We present two ways to determine this time limit. The first way is to analyze the distribution of the INC stage time. Beyond this time, there are no more quasifree hadrons inside the nucleus including Δ resonances. Distributions of this INC stage time are shown for six incident energies of proton induced reaction on ^{208}Pb in Fig. 2. For each reaction, a large peak appears below 100 fm/c and a tail spreads to late times. The peak goes to a lower time as the incident energy increases, this is due to peripheral collisions (high impact parameter b of incident particle) which give faster nonelastic events when energy increases. We notice a clear change of slope around 80–100 fm/c. At large times, the INC stage ends when the last quasifree hadron is either emitted or absorbed into the gap above the local Fermi energy $e_F(r)$ after a last collision allowed by Pauli blocking (*quasifree* + *bound* → *bound* + *bound* transition) or after a last Δ decay. In the case of emission at large time, the nucleon leaves the nucleus with a low kinetic energy and the excitation energies U_{exc} and E_{exc} change slightly. This is confirmed by the small change of the mean value of the two excitation energies above 100 fm/c in Fig. 1.

The second way to determine the time limit of the INC stage is to compare the distributions of the two excitation energies $U_{\text{exc}}(t)$ and $E_{\text{exc}}(t)$ rather than their mean values. Figure 3 shows the distributions of the excitation energies defined by the expressions (22) and (23) at six times for the 800 MeV proton induced reaction on ^{208}Pb. The distributions present no more large changes after 100 fm/c, which means that nucleons emitted at large times have a small outgoing energy. However, we notice that the distribution $U_{\text{exc}}(t)$ does not change much above 75 fm/c, while $E_{\text{exc}}(t)$ still changes after 100 fm/c. Thus, the absorption of the last quasifree hadrons in the bound system (*quasifree* + *bound*→*bound* + *bound* transition) is the main process that governs the small evolution of $E_{\text{exc}}(t)$ after 75–100 fm/c without changing the distribution of U_{exc}.

The comparison of the two excitation energies $U_{\text{exc}}(t)$ and $E_{\text{exc}}(t)$ and the distribution of the INC stage time allows us to define the time cut t_{cut} to end the cascade stage (when there is still at least one quasifree hadron in the updated nucleus). We verified that the distributions of $U_{\text{exc}}(t_{\text{cut}})$ at time $t_{\text{cut}} =$ 100 fm/c are similar to the same distributions at higher times for the 40–1600 MeV energy range and for target nuclei defined with $\epsilon_\rho \geqslant 0.005$ (t_{cut} has to be increased if ϵ_ρ decreases). That choice has already been done by the authors of Refs. [32,33] for the QMD model to describe the first stage of the nonelastic reactions induced by protons.

We point out that the definitions of our INC stage time and of the equilibration time in the QMD model of Ref. [58] are similar. Indeed, the two times are overall times that include the time of the incident hadron to enter the nucleus, the times of successive collisions, and the times for quasifree particles to reach the edge of the nucleus. However, our INC stage time is determined more easily than the time of equilibration is estimated for the QMD model. In the QMD model, there is no separation between hadrons: all nucleons and other hadrons are moving according to the equations of motion derived from the QMD Hamiltonian; and there should not be an easy way to separate nucleons between quasifree nucleons and bound nucleons. The time of equilibration defined in Ref. [58] is based on the shape of neutron spectra near the evaporation component, while our INC stage time is easily defined event by event when quasifree hadrons are gone from the nucleus. Defining this time would have been difficult if we had included collisions between bound nucleons.

The time cut $t_{\rm cut}$ could be lowered for high energy reactions on light nuclei; however, our approach based on the freezing of bound nucleons forbids the evolution of the preresidual nucleus and then the emission of the nucleon as in a pseudoevaporation stage. In our model, a higher $t_{\rm cut}$ would provide statistically similar results than with $t_{\rm cut} = 100$ fm/c. This time cut is more a numerical parameter than a physical parameter, like the time step Δt. Its aim is to end the INC stage of the nonelastic event, since we cannot prevent a quasifree hadron from wandering in the nucleus a very long time (on some internal orbiting trajectory due to equations of motion). Nevertheless, it has to be high enough to complete the INC stage. The particular case of reactions induced by low energy neutrons (10–30 MeV) is discussed in Sec. III B6.

At time $t_{\rm cut}$, the excitation energy includes the energy of all Δ's and pions that remain inside the nuclear volume and the mass excess balance. It is then simply the total excitation energy $U_{\rm exc}(t_{\rm cut})$, and the excited nucleus at time $t_{\rm cut}$ is the preresidual nucleus plus the remaining quasifree hadrons inside it; this is therefore the updated nucleus.

III. CALCULATIONS AND DISCUSSION

A. Framework of calculations

In spallation studies, most of the experimental data at a given energy may be divided into two classes: the production cross sections of particles and nuclei and the differential cross sections or spectra of particles. They depend on the two stages of the reaction, the INC and the deexcitation steps. However, the differential cross sections of particle production provide more information on the dynamics of the reaction than do the yields of nuclei production. Moreover, the production of nucleons of energy above the evaporation region and the production of the pions are two outputs that come exclusively from the fast stage, the INC in our case. The production yields of residual nuclei are the final result of the deexcitation stage after the INC calculation. Even if they depend on the outputs of the INC (excitation energy, mass, charge and angular momentum of the remaining nucleus at the end of the cascade), their dependence on the physics and on the parameters of the evaporation and fission models is strong. The same remark can be made about the production of evaporated particles.

To focus on the physics of the INC stage in this paper, we restrict our comparisons to the double differential cross sections of nucleon production in the continuum, paying particular attention to the region of high outgoing energy (typically above 25 MeV). The particle production of outgoing energy below 25 MeV provides information on the behavior of the full reaction, the INC and the deexcitation. Neutron production in this energy region gives some indication of whether the excitation energy at the end of the INC step is too high or not.

In fact, since our present INC model does not treat the emission of light nuclei (deuterons, tritons, α's, etc.), we will present the production of the "primordial" nucleons [7] in the first stage of the reaction. One has to keep in mind that the calculated nucleon production should be slightly reduced to feed cluster production. Experimental measurements [19,59,60] show that cluster production is small compared with nucleon production in most of the measurements. Deuteron and α production, however, may not be negligible in low intermediate energy reactions [19] because of the pickup and knockout processes, respectively. Nevertheless, we will assume that the production of primordial nucleons above the evaporation energy area is close to the real production of nucleons in the first approximation, at least above 80 MeV incident energy.

We now detail the framework of the calculations. When experimental data of differential cross sections extend down the evaporation area, our calculations will include the contribution of the deexcitation stage.

1. Deexcitation stage

Our evaporation code is based on the statistical theory of Weisskopf and Ewing [61]. The calculation of the partial width Γ_i of each emitted particle ($i = p, n, d, t, {}^3\mathrm{He}, \alpha$) is done in the following way. The level density functions come from the model of the back-shifted gas of independent fermions and use the energy-dependent level density parameter of Ignatyuk *et al.* [62]. The inverse cross sections of Γ_i are assumed to be the reaction cross sections. They were calculated in our laboratory [38] with an optical model for neutrons up 20 MeV, with a geometrical model fitted on experimental data up to 10–30 MeV/A above the Coulomb threshold for light charged particles. Above these energies, reaction cross sections come from a Glauber model which uses the matter density distribution of nuclei from the HFB calculation [39].

The deexcitation of excited heavy nuclei includes the competition between the evaporation and fission processes. The RAL model of Atchison [63] is used to compute the probability of fission at each step of the deexcitation stage and, when fission occurs, to determine the mass, charge, and energy of the daughter nuclei after scission. Since the parametrizations of the ratio of fission and neutron partial widths Γ_f/Γ_n were adjusted with another evaporation code, they were not consistent with our evaporation. A phenomenological scaling factor equal to 0.3 has then been applied to the fission probability of the RAL model to give reasonable fission cross sections of lead on a wide range of incident energy. After scission, the two daughter nuclei follow their own evaporation chain.

Light nuclei [$A_{\rm upd}(t_{\rm cut}) < 30$] with total excitation energy greater than predefined energy levels are dealt with using a statistical model of fragmentation called "Fermi breakup" based on microcanonical theory [64,65].

To compare calculations with thick targets measurements, we present in Sec. III B either the INC results, if experimental data are available only above the evaporation area, or the results of INC plus evaporation/fission/fragmentation, otherwise. When the thickness of the target in the experimental setup is not negligible, the TIERCE code system [66] is used to simulate transport in the experimental target of all particles except neutrons below 19.6 MeV with our modified HETC code and the transport of neutrons below 19.6 MeV with MCNP [25]. The reaction cross sections of the high energy transport are those of the evaporation code. Several INC models are available in our

TABLE I. Differences between BRIC versions 1.0 and 1.4.

	BRIC 1.0	BRIC 1.4
Potential	$V(r) = V_0(A)\,.\,[(\rho(r)/\rho_0)^{2/3} - e_{\text{bind}}]$	$V(r)$ from Eq. (6)
	$V_0(A)$ increasing with mass A	$V_0 = -48$ MeV
	No V_{Coulomb}	V_{Coulomb} from uniform charge distribution
Equations of motion of quasifree hadrons	$d\vec{p}/dt$ not defined (no refraction)	$d\vec{p}/dt = -\vec{\nabla}\,V$
	$d\vec{r}/dt = \vec{p}/E$	$d\vec{r}/dt = \vec{p}/E$
NN cross section	Fit on experimental cross sections	In-medium cross section below 500 MeV [Eq. (12)]
Q value	Not taken into account	Taken into account
Transmission coefficient	Gamow factor [46] with $V(r)$	WKB calculation with $V(r)$

HETC: Bertini's (code MECC-7) and two versions of our cascade code BRIC. The selected INC model followed by deexcitation is thus the generator of nonelastic events in HETC.

2. *Short description of older* BRIC *version*

In the next section, we compare the results of our current version BRIC 1.4 with experimental data, sometimes with the INC model of Bertini, and systematically with an older version, BRIC 1.0. This old version has been described in Ref. [34]. We detail briefly the main differences between the two versions. They are listed in Table I.

In BRIC 1.0, the potential is

$$V(r) = V_0(A)\left[\left(\frac{\rho(r)}{\rho_0(A)}\right)^{2/3} - e_{\text{bind}}\right],$$

where the amplitude $V_0(A)$ of the potential well increases linearly with the mass number A through $V_0(12) = -32.5$ MeV and $V_0(208) = -45$ MeV. The shift $-e_{\text{bind}}$ was applied to ensure that all the nucleons are bound. The protons, neutrons, and Δ's share the same potential, but the pions have no potential. The Coulomb potential is not included in $V(r)$. However, it enters the calculation of the transmission coefficient of quasifree charged hadrons as they are going to leave the nuclear volume. The probability of reflecting a charged hadron back inside the nucleus is given by a Gamow factor as in Ref. [46] with our potential $V(r)$. The different definitions of $V(r)$ produce also a different local Fermi energy $e_F(r)$ between the two versions, mainly for protons due to the lack of Coulomb potential, and for light and medium target nuclei.

In BRIC 1.0, refraction is not taken into account. Since the potential $V(r)$ is a smooth function of position r, the equations of motion may not be easily read. The energy $E_i + V(r_i)$ of a hadron i is conserved when it moves from one point $\vec{r}_i$ to another $\vec{r'}_i$, but the momentum direction is not changed in the motion. This approximation is justified for a constant potential $V(r) = V_0(A)$ or for high energy hadrons. However, it was chosen to minimize the computing time. Moreover, it affords a direct comparison with the INC of Bertini where the motion of hadrons is done in the same way.

The parametrizations of the nucleon-nucleon elastic and total cross sections are fitted on experimental data since we have assumed in BRIC 1.0 that they are the free ones in the nucleus. To finish, the Q value is not taken into account in the first pn collision, thus the outgoing energy distributions of the (p, xn) and (n, xp) reactions go up to the incident energy.

BRIC versions 1.4 and 1.0 share the same numerical algorithms of the initialization and of the collision term (despite their respective default NN elastic cross sections), but they have different numerical algorithms of transport inside the nucleus, because they were optimized independently to reduce their respective computing times. Some interchanges are nevertheless possible, mainly in the collision term. That will allow us to show the effects of refraction and of the in-medium NN cross sections.

3. *Calculation of reaction cross section*

The differential cross sections are calculated according to

$$\frac{d^2\sigma}{dE\,d\Omega} = \frac{\sigma_R}{N_{\text{non-el}}}\frac{\Delta^{(2)}N}{\Delta E(2\pi\,\Delta\cos\theta)},$$

where ΔE and $\Delta\cos\theta$ are the bin sizes of the outgoing energy and of the emission angle from the beam direction, in the distribution, respectively. $\Delta^{(2)}N$ is the number of particles that obey the criteria on observables $(E_{\text{obs}} - \Delta E/2 < E < E_{\text{obs}} + \Delta E/2$ and $\theta_{\text{obs}} - \Delta\theta/2 < \theta < \theta_{\text{obs}} + \Delta\theta/2)$. $N_{\text{non-el}}$ is the number of nonelastic events among the total number of events N_{tot}. A nonelastic event occurs when the energy of at least one bound nucleon of the target nucleus changes in the event. σ_R is the nonelastic reaction cross section. It may be given by an independent model such as an optical model or a Glauber model at high energy, by a systematics, or by the INC model itself. We use the code BRIC to compute this nonelastic cross section according to

$$\sigma_R = \frac{N_{\text{non-el}}}{N_{\text{tot}}}\sigma_{\text{geo}},$$

where σ_{geo} is the geometrical cross section corresponding to the maximal impact parameter b_{max} of the incident particle. In the present paper, $b_{\text{max}} = R_{\text{limit}}$, and it depends on the atomic mass A through the radius $R_m(A)$ and the diffusiveness $a(A)$ of the nucleus.

The ratio is averaged on a large number $N_{\text{non-el}}$ of nonelastic reactions, between 1.6×10^6 (heavy target nuclei) and

TABLE II. Reaction cross sections calculated by BRIC versions 1.0 and 1.4 for the reactions presented in this paper. These values were used to normalize double differential cross section calculations shown in Figs. 4–17 and 20–22. OMP K-D are the results of the global optical model potential of Koning and Delaroche [67].

Target	Energy (MeV)	σ_R (mb)		
		BRIC 1.0	BRIC 1.4	OMP K-D
	Incident proton			
^{90}Zr	45	1357	1443	1308
^{208}Pb	45	2235	2453	2000
^{54}Fe	62	908	918	886
^{93}Nb	65	1261	1340	1233
^{90}Zr	80.5	1140	1180	1138
^{208}Pb	80.5	1978	2168	1979
^{58}Ni	100	774	770	790
^{197}Au	100	1781	1931	1841
^{27}Al	113	436	404	449
^{238}U	113	2040	2196	2020
^{90}Zr	120	987	978	1018
^{208}Pb	160	1689	1679	1742
^{58}Ni	200	689	582	656
^{197}Au	200	1612	1522	1618
^{27}Al	256	393	321	348
^{238}U	256	1903	1761	1777
^{9}Be	300	170	130	–
^{107}Ag	300	1066	971	–
^{40}Ca	392	523	481	–
^{58}Ni	400	691	647	–
^{56}Fe	597	734	692	–
^{208}Pb	597	1761	1688	–
^{208}Pb	730	1805	1714	–
	Incident neutron			
^{209}Bi	14	1958	2293	3054
^{238}U	18	2373	2817	3290

3×10^6 (light target nuclei), or up to 5×10^6 if necessary, to get reasonable statistics in the calculation of double differential cross sections.

The nonelastic cross sections σ_R that normalize the differential cross sections of the two calculations BRIC 1.0 and BRIC 1.4 of this paper are given in Table II. Reaction cross sections from the global optical model potential of Koning and Delaroche (OMP K-D) [67] are also presented in the right column for incident energies below 256 MeV. We notice that BRIC 1.4 results and those of the OMP are within 10% except for the reactions on the higher target masses at lowest energies, below 60 MeV. This discrepancy is due to some approximations applied to the incident particle at the initialization in our approach, and they will be suppressed in a future version.

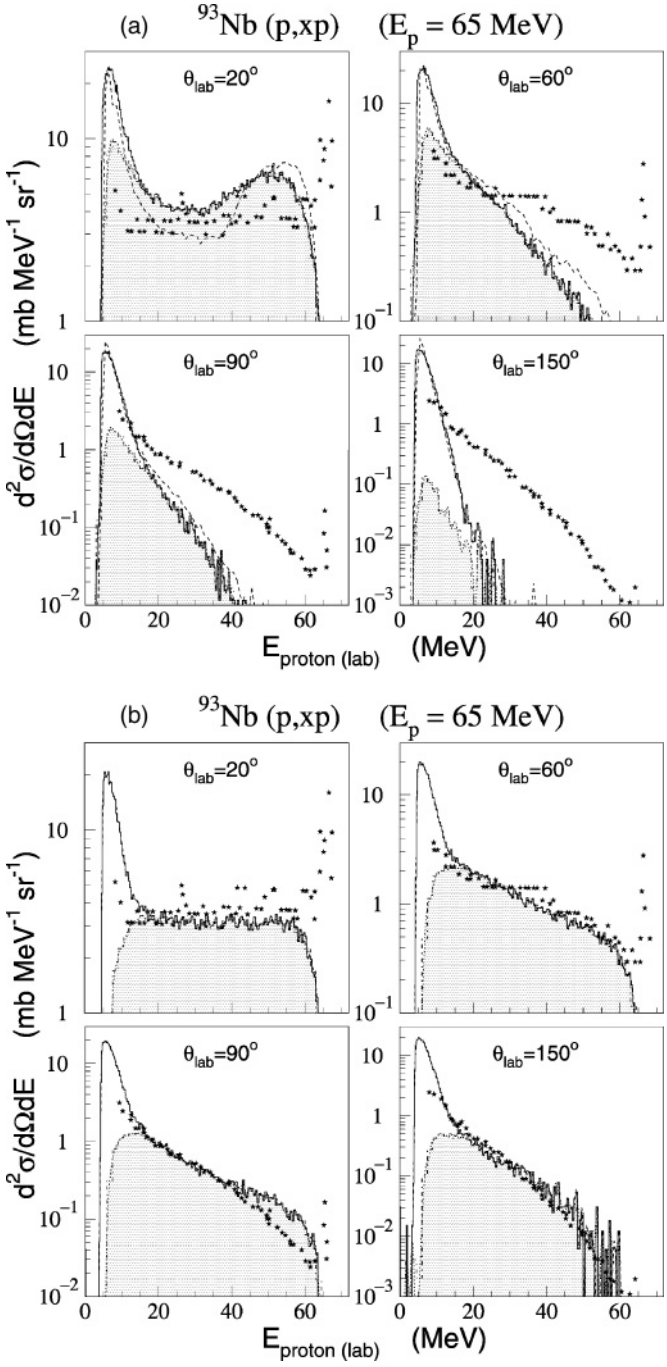

FIG. 4. Differential cross section of proton production for reaction of 65 MeV proton on ^{93}Nb as a function of the outgoing proton energy for the angles indicated. Results are from (a) BRIC 1.0 and (b) BRIC 1.4. Filled area is the INC component of our model; solid histogram is the INC + evaporation sum. Hashed line in (a) is the result of the sum of Bertini's INC plus evaporation. Symbols are data of Sakai *et al.* [68].

B. Comparison of results

Figure 4 shows the double differential cross section of proton production for the reaction of a 65 MeV proton on ^{93}Nb. In panel (a) we present the results of BRIC 1.0 only (filled area), of BRIC 1.0 and evaporation (solid histograms) and of MECC-7 and evaporation (hashed line). We notice that the results of BRIC 1.0 are similar to those of MECC-7. Although these INC models differ on some points (no time approach is used in Bertini's INC and the nuclear density of the target nucleus is a smooth function in our model, for instance), they include, however, the

same rough approximations that produce on average the same kind of discrepancies: an overproduction of emitted protons at forward angles in the range of high emission energy often called the quasielastic "peak" and too few protons produced at backward angles. At 20°, the saddle shape is more pronounced with MECC-7 than with BRIC 1.0; that certainly comes from the density distribution described by three concentric spheres in the Bertini's model. At very backward angles, the contribution of the INC step is almost negligible in comparison with the evaporation step: proton production is strongly decreased above 20 MeV at 150°, for instance. These discrepancies have already been observed in previous studies [17–19]. Another characteristic of such an INC model, without refraction or in-medium NN cross sections, is a peak in the area of low outgoing energy at forward angles. However, when compared with experimental data, this peak is more difficult to identify, because it stands in the energy range of evaporated particles. This peak comes mainly from the peripheral nucleon-nucleus collisions, where the incident or struck nucleon has a small energy after collision (enough to go out of the nucleus). In these reactions, forward angles are favored by the incident momentum and kinematics. This is the counterpart of the quasielastic peaks (p, p') and (p, n) at high outgoing energy. We will show that the overproduction of low emission energy particles at forward angles that appears systematically with such INC models (MECC-7 and BRIC 1.0 in this paper) can be suppressed when the refraction and in-medium NN cross sections are taken into account, as is the case in BRIC 1.4.

Figure 4(b) shows the results of our current model. The calculations are clearly in better agreement with the data for the four angles. The distribution of outgoing protons in the INC step is flatter at forward angles, and the peaks at 20° of the low and high energy protons have vanished. At backward angles, the contribution of the INC is no longer negligible above the area of the evaporated protons (above 20 MeV).

Figure 5 shows the same results for the ^{54}Fe(p, xp) reaction at 62 MeV. This reaction is similar in energy to the previous one but for a lighter nucleus and with more detection angles that extend down to 12°. We see again the same changes in the double differential cross sections of outgoing protons for BRIC 1.4 [Fig. 5(b)] when compared with those for BRIC 1.0 [Fig. 5(a)]: a flat distribution at forward angles instead of a peaked one, and a higher INC component at very backward angles instead of a negligible one. The distributions obtained by our present model are also in good agreement with data at the intermediate angles. Nevertheless, the calculation with our current model presents a discrepancy at very forward angles (below 20°): while the distribution is almost correct in shape, except for the structure due to nuclear levels, the calculated yield of outgoing protons is underestimated. Comparisons with other data of the same experiment [17] confirm the presence of this discrepancy that appears at very forward angles, at least at this incident energy. It is not visible with other experiments, but it is certainly because of their angular limitations. No particular reason for this discrepancy has been identified. We only may point out that the differential cross sections of elastic nucleon-nucleon scattering used in BRIC 1.4

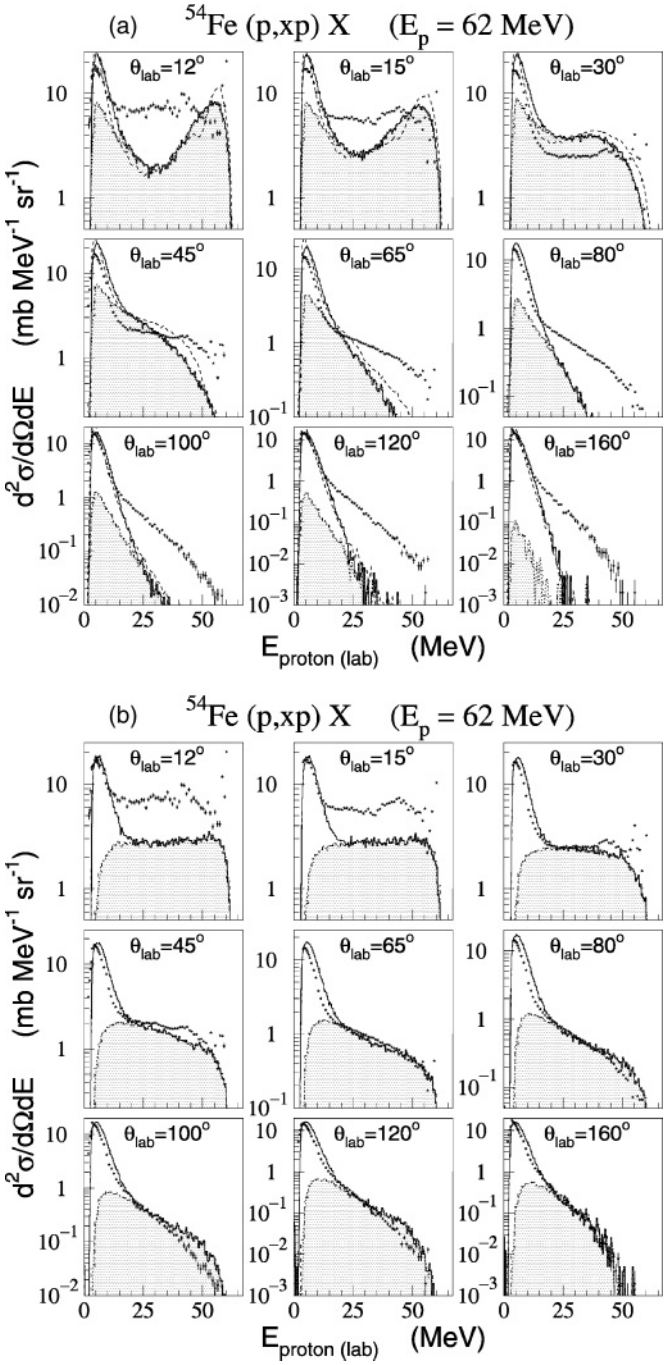

FIG. 5. Same as in Fig. 4, but for 62 MeV proton on ^{54}Fe. Data are from Ref. [17].

are not the in-medium ones, but the free ones, then it may influence the angular differential cross section of outgoing nucleon.

Before showing and discussing the results at higher energies, we present separately the effects of the in-medium NN elastic cross sections and of the realistic equations of motion. To do that, we compare calculations with data for the proton induced reactions on ^{90}Zr at 45 and 80 MeV in panels (a) and (b), respectively, of Figs. 6–8.

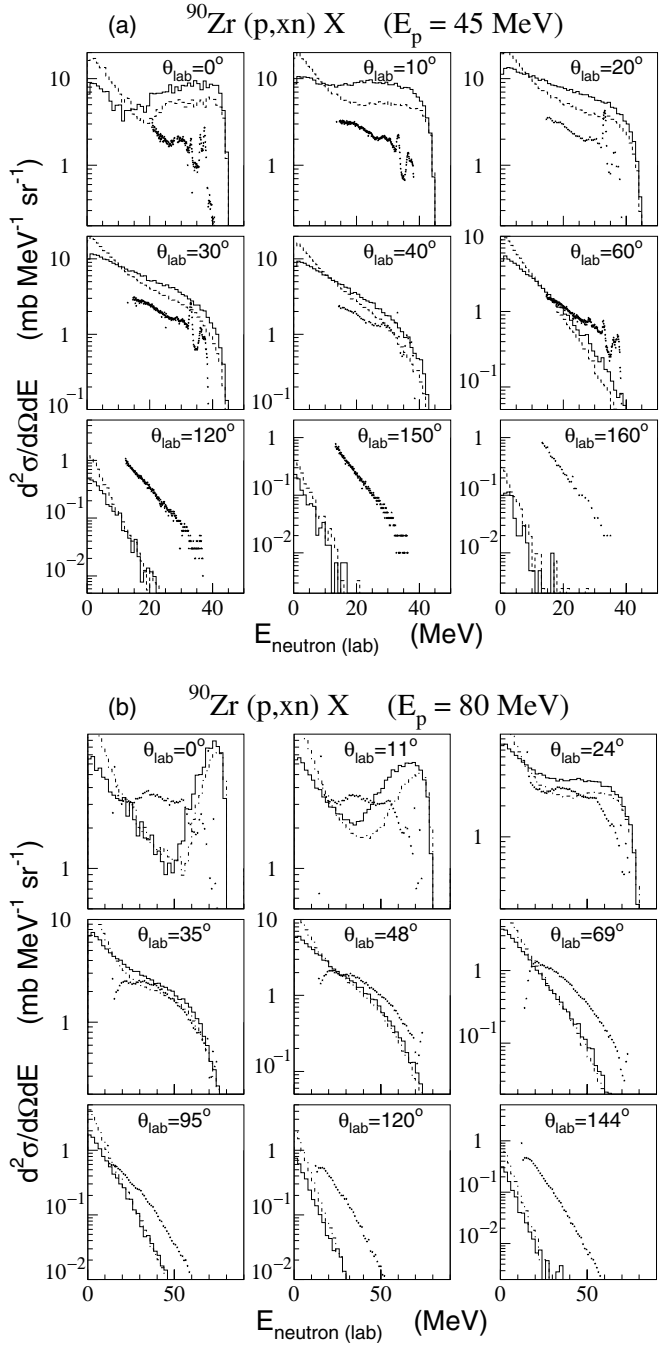

FIG. 6. Double differential cross sections of neutron production in ^{90}Zr(p, xn) reaction at (a) 45 MeV and (b) 80 MeV. Symbols are data from Ref. [69] (45 MeV proton) and [70] (80 MeV proton). Hashed histograms are the results of BRIC 1.0; solid histograms, BRIC 1.0 with the in-medium NN elastic cross sections [Eq. (12)]. Evaporation component is not included.

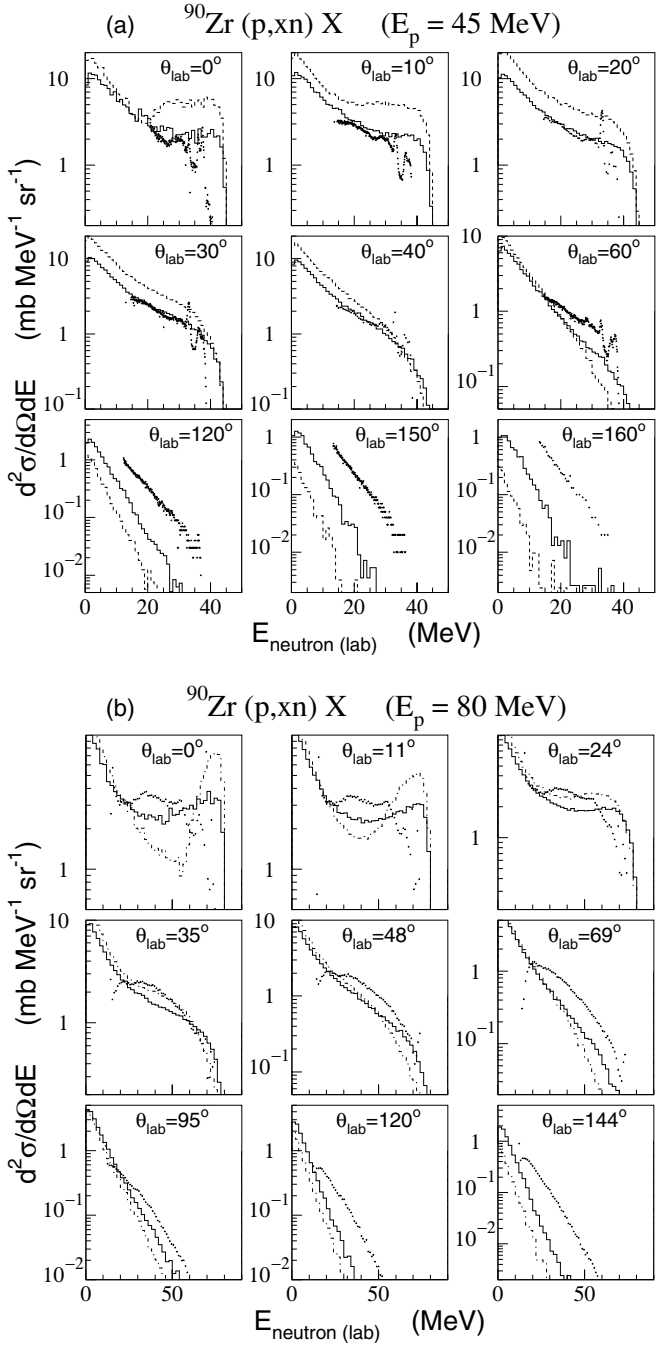

FIG. 7. Same reactions as in Fig. 6, but showing results for BRIC 1.0 (hashed histograms), and BRIC 1.4 with the free NN elastic cross sections and without taking into account $Q(p, n)$ (solid histograms).

1. *Effect of the in-medium cross sections*

In Fig. 6, hashed histograms are the results of BRIC 1.0 and solid histograms are those of BRIC 1.0 in which free NN elastic cross sections were replaced by the parametrizations of the in-medium cross sections (12). The production of higher energy protons is slightly increased at forward angles in the two reactions. This can be explained by the increase of the mean free path of quasifree nucleons in the nucleus when the in-medium NN cross sections are used. In that case, a quasifree nucleon has a higher probability of leaving the nucleus after only one collision. Since there is no refraction, outgoing nucleons leave the nucleus mostly in the forward direction. We also notice that the yield and slope of the distribution of low energy outgoing neutrons (evaporation area) are smaller.

However, using the in-medium cross sections instead of the free NN cross sections in BRIC 1.0 does not really improve

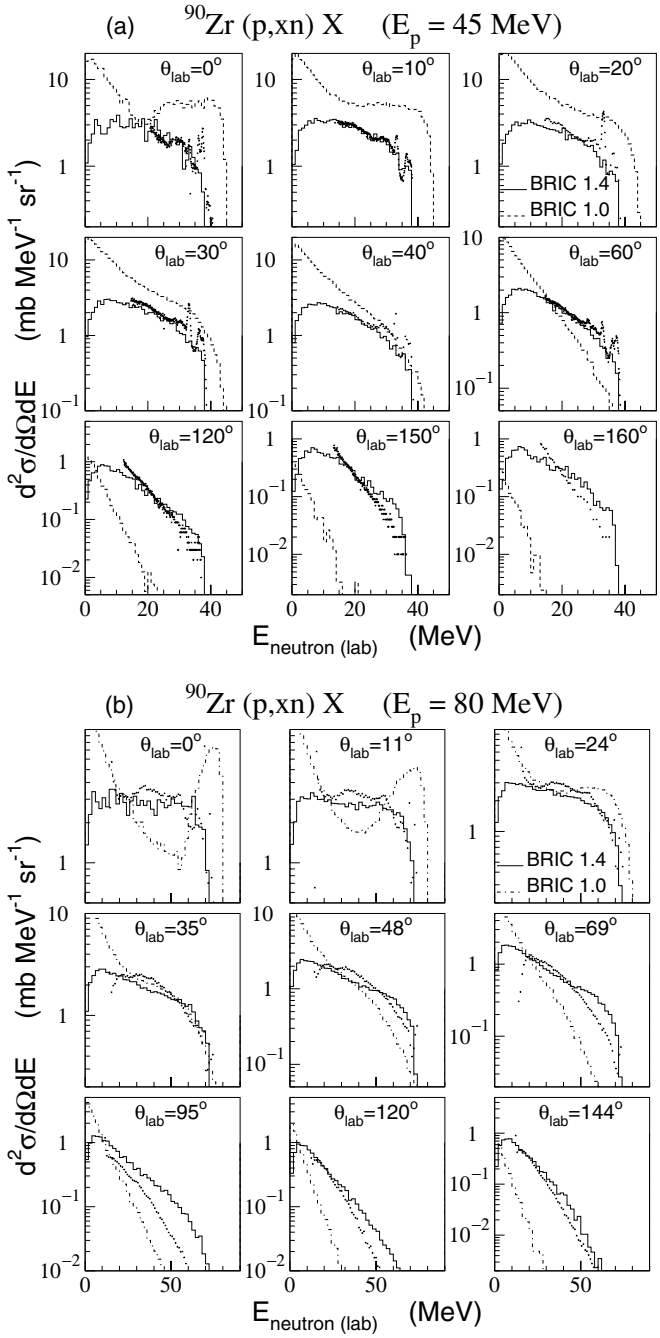

FIG. 8. Same as in Fig. 7, but with our current BRIC 1.4.

the results above the evaporation area. They even get worse at forward angles for these two reactions.

2. *Effects of the equations of motion*

To identify the effects of the refraction only, we compare the results of BRIC 1.4 with free NN elastic cross sections and without the Q-value shift to the results of BRIC 1.0 (Fig. 7). The effect of the refraction depends on the energy of the incident proton and on the emission angle of the outgoing neutrons. At 45 MeV, on the one hand, it decreases the neutron production at forward angles without changing the shape of the distribution; on the other hand, the production of backward neutrons is increased. At 80 MeV, the refraction effect appears more clearly for high energy neutrons at forward angles: the quasielastic peak is decreased and the energy distribution of neutrons is more constant when refraction is applied (solid histograms). We already observed this characteristic for proton production in reactions around 65 MeV [Figs. 4(b) and 5(b)]. Moreover, the increase of neutron production in the backward direction is smaller at 80 than at 45 MeV.

Figure 8 presents the results of BRIC 1.4 (solid histograms) and of BRIC 1.0 (hashed histograms). As the Q value is taken into account in BRIC 1.4 in the pn collision, the maximal outgoing neutron energy at forward angles is lower in comparison to BRIC 1.0 results. The shape of the outgoing neutron energy distribution from our present model is on the whole in good agreement with the data, and the yields are close to data within a factor of 2 or less. The large discrepancies at very forward and backward directions given by BRIC 1.0 are strongly attenuated at the least, or even disappear. Figure 9 shows similar results for proton induced reactions on ^{208}Pb at the same energies. At 45 MeV, we notice that INC is not able to reproduce the fine structures of the differential cross sections such as the large isobaric analog resonance in ^{208}Pb(p, xn) at forward direction. Indeed, the bound nucleons are distributed in phase space according to a continuous Fermi gas, and no nuclear level of the target nucleus is taken into account. Moreover, our present INC model does not succeed in reproducing well the extremity of the spectra at forward direction [Fig. 9(a)] even if the $Q(p, n)$ value for reactions on ^{208}Pb is lower than for reactions on ^{90}Zr. That failure is certainly due to the simplified description of the nucleus and the semiclassical approach of the collision term.

A more realistic treatment of the dynamics for the quasifree nucleons, i.e., the refraction, has a significant effect on the distribution of lower energy outgoing nucleons and at low incident energy, as we would expect. However, refraction is not sufficient to provide good agreement with experimental data on the whole angular range. The results are in better agreement in forward and backward directions only when we combine equations of motion and in-medium NN cross sections.

3. *Reactions from 100 to 500 MeV*

Figures 10(a) and 10(b) show the double differential cross section of neutron production for the reactions of protons on ^{90}Zr at 120 MeV and on ^{208}Pb at 160 MeV, respectively. We see the same agreement between the results of BRIC 1.4 (solid histograms) and data in forward and backward directions as previously. These are clear improvements over the results of our older INC model (hashed histograms). However, at intermediate angles of forward direction (24°–82°), outgoing neutrons of higher energy are overestimated in BRIC 1.4 calculations, contrary to BRIC 1.0 calculations. We will come back later to this discrepancy, which does not exist at lower incident energy (see Figs. 8 and 9).

Comparisons with the data of Meier *et al.* at 113 [20] and 256 MeV [21] for the ^{27}Al target in Fig. 11 and for the ^{238}U target in Fig. 12 include the calculations done with Bertini's

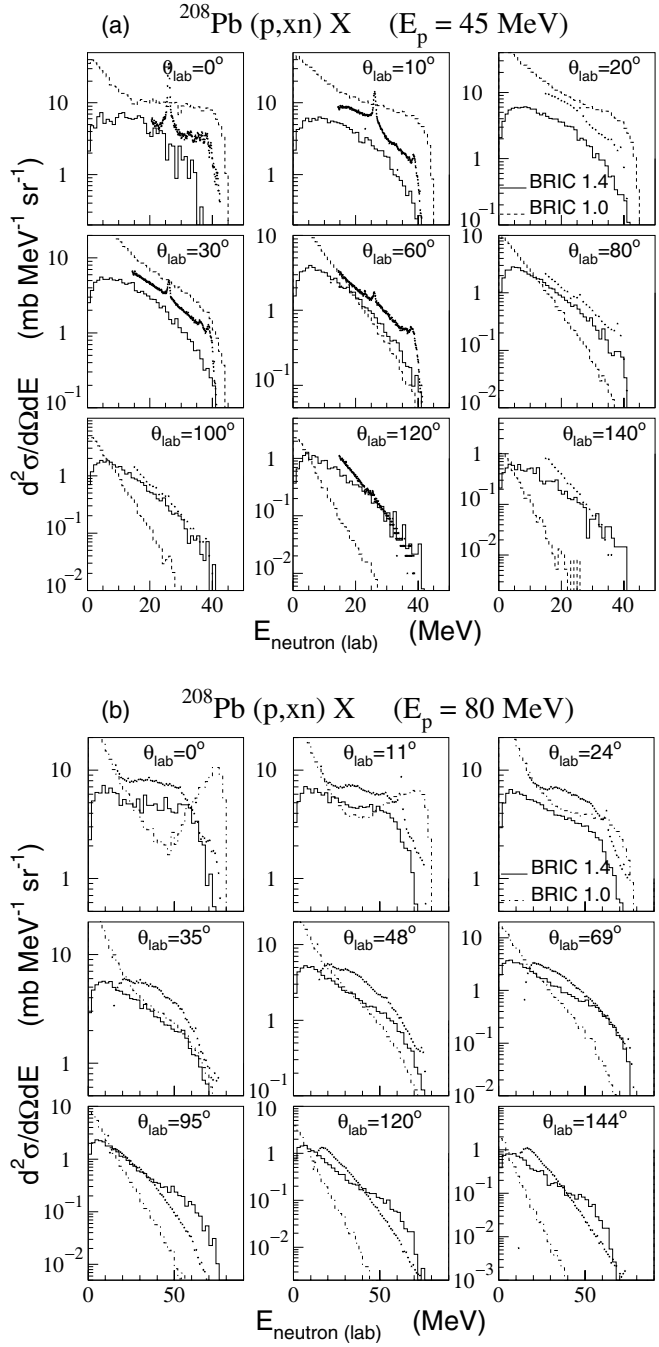

FIG. 9. Same as in Fig. 8, but for proton induced reactions on ^{208}Pb. Symbols are experimental data of (a) Galonsky *et al*. [19] and (b) Cowley *et al*. [71].

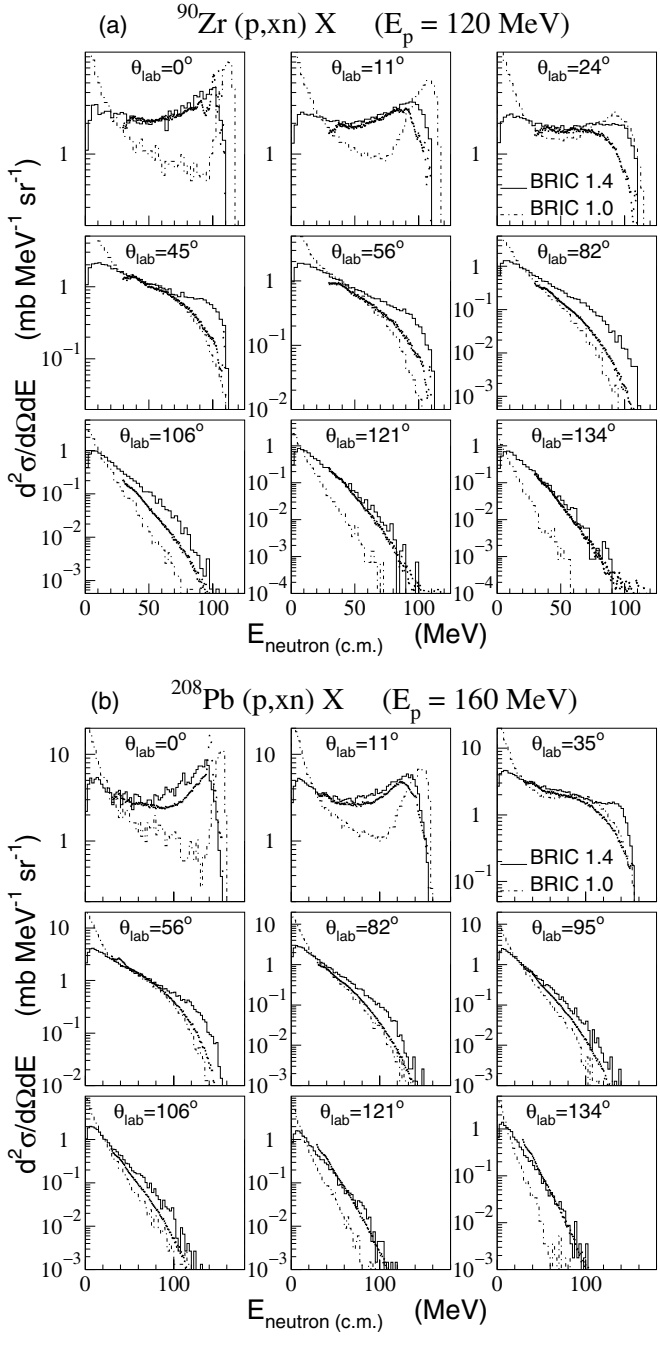

FIG. 10. Differential cross section of neutron production for the reactions (a) ^{90}Zr(p, xn) at 120 MeV and (b) ^{208}Pb(p, xn) at 160 MeV as a function of the c.m. energy of the outgoing neutrons for the indicated laboratory angles. Results of BRIC 1.4 (no evaporation) (solid histograms) and BRIC 1.0 (hashed histograms). Experimental data (stars) are from Ref. [72].

INC model. The latter were normalized by the reaction cross section σ_R of BRIC 1.0 to make the comparison between these two models easier. Their results are very close in shape and yields, or at least within a factor of less than 2. Thus they produce the same discrepancies as we have already seen for proton production in proton induced reactions around 60 MeV (Figs. 4 and 5). Moreover, we notice that their respective evaporation components are globally the same. On the other hand, the results of BRIC 1.4 are in better agreement at three places: at 7.5° the energy distribution above the evaporation area is better in shape and less than a factor 2 from data in yields; there is less underproduction at backward angles; and there is good agreement with data at the forward direction in the evaporation area. This last point comes from a lower yield of low energy outgoing neutrons in our present INC model than in our older version, as we have already explained. The calculations without the evaporation stage in Fig. 10 confirm

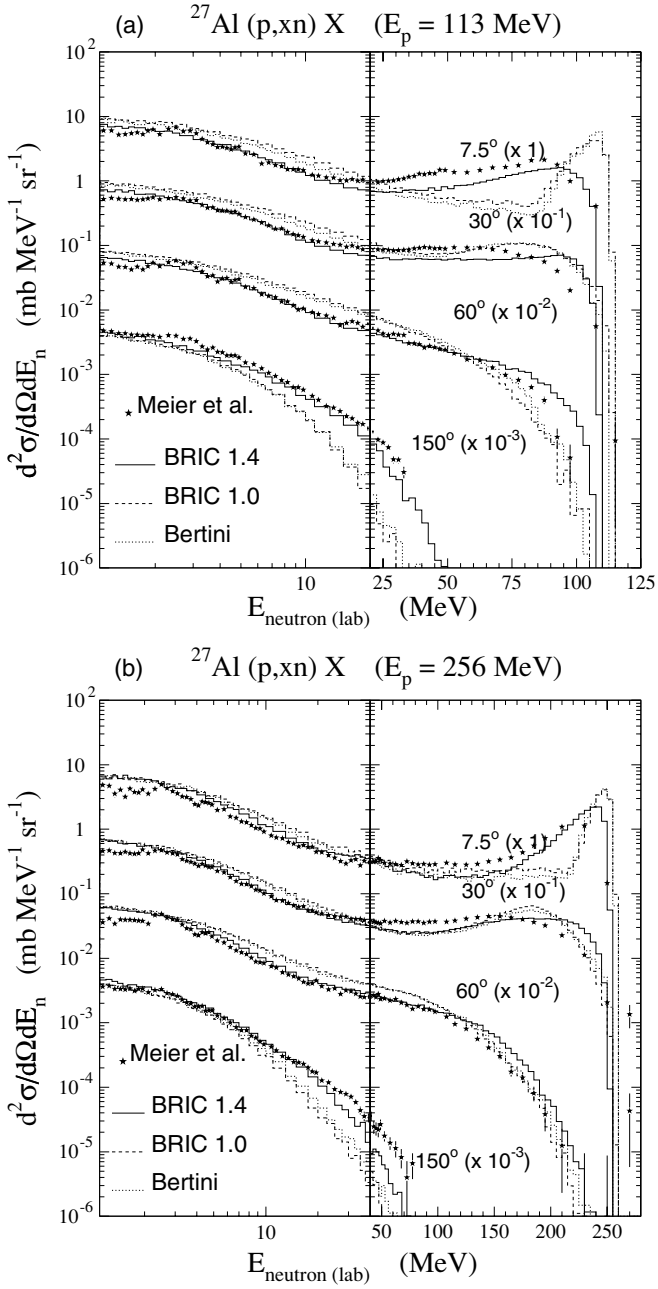

FIG. 11. Differential cross section of neutron production for the reactions ^{27}Al(p, xn) at (a) 113 MeV and (b) 256 MeV as a function of the energy of the outgoing neutrons for the angles indicated in the laboratory frame. The results at two successive angles are shifted by a 0.1 factor. The solid, hashed, and dotted histograms are the results of BRIC 1.4, BRIC 1.0, and Bertini's INC, respectively, plus evaporation. Data at 113 and 256 MeV are from Refs. [20] and [21], respectively.

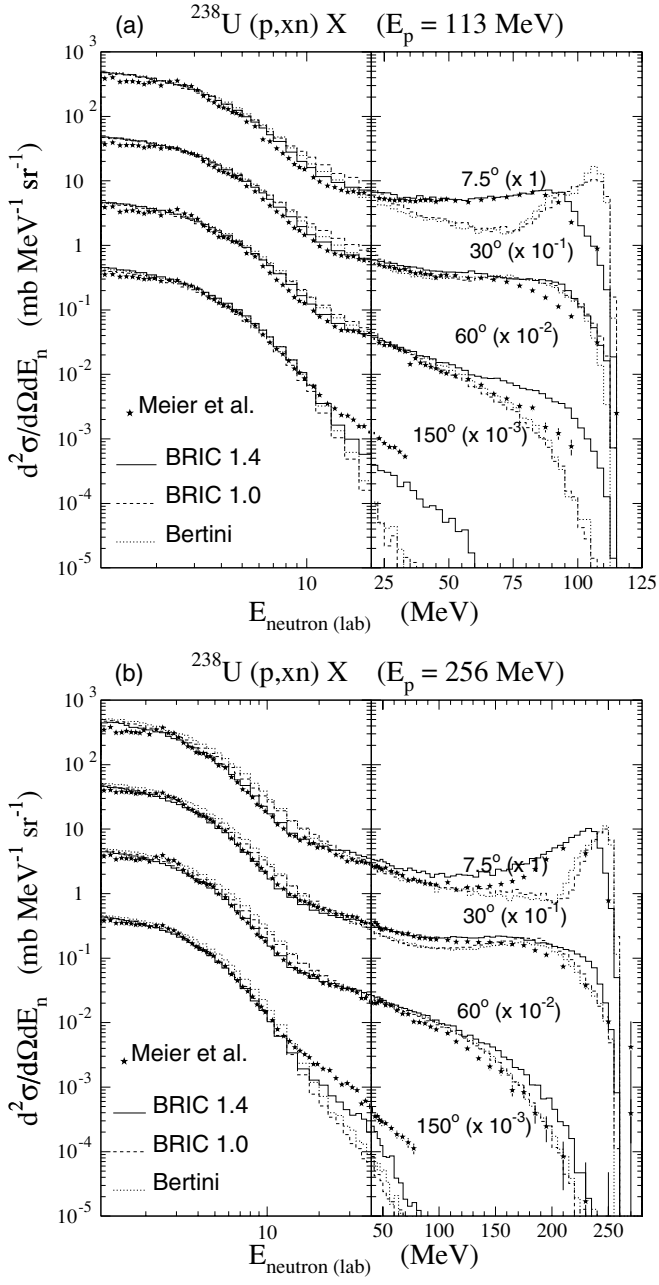

FIG. 12. Same as in Fig. 11, but for ^{238}U(p, xn).

that the production of neutrons of energy lower than 25 MeV is much less at the forward direction with BRIC 1.4 than with BRIC 1.0. However, as we have also noticed in this figure, higher energy neutrons at 30° and 60° are overestimated. Before discussing this discrepancy, we will see energy distributions of outgoing protons, still for proton induced reactions for incident energies between 100 and 400 MeV.

Looking at differential cross sections as a function of the angle of the outgoing nucleon (Figs. 13 and 14), distributions at high outgoing energy E_{out} become progressively more peaked to the forward direction as the incident energy E_{inc} increases. Although the distributions calculated by our older INC are much too peaked, this trend is well reproduced by BRIC 1.4 for proton emission in the reactions $p + ^{58}$Ni at 100 and 200 MeV (Fig. 13) and $p + ^{197}$Au at 100 and 200 MeV (Fig. 14). This agreement with data is confirmed for other intermediate energies (120, 150, and 175 MeV) and for other target nuclei [74,75]. At 100 MeV, the production of outgoing protons at backward angles is in substantially better agreement for BRIC 1.4 than for BRIC 1.0. The difference between the two versions diminishes with increasing incident

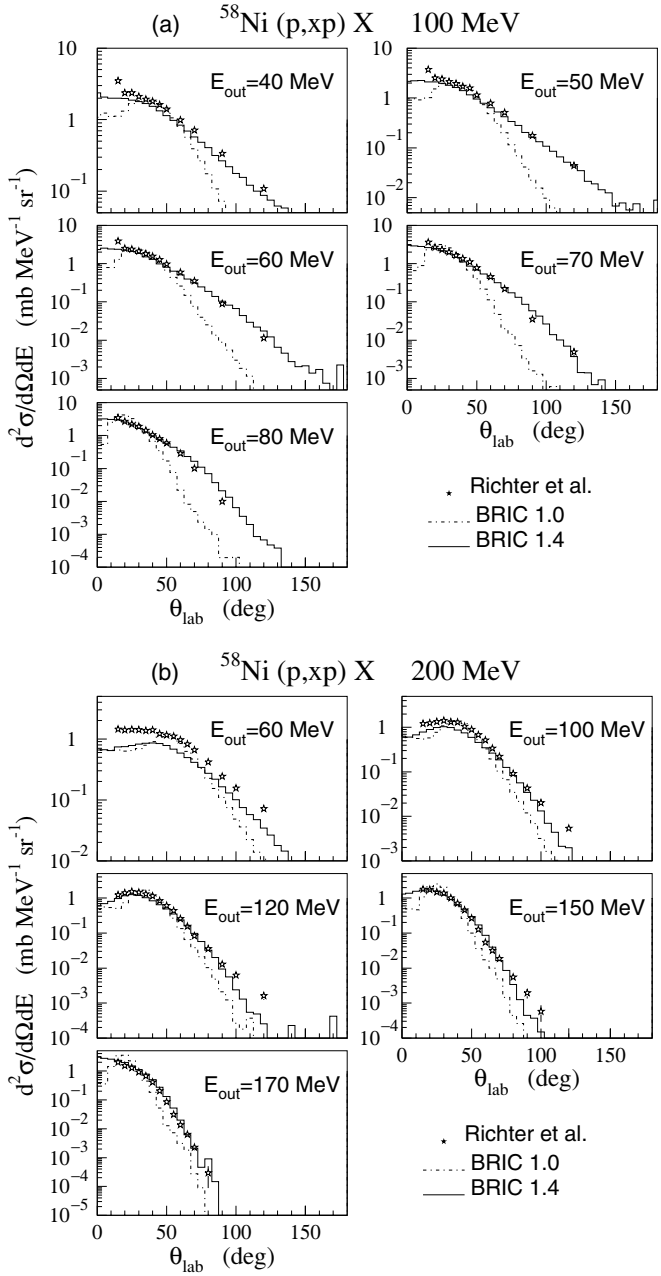

FIG. 13. Differential cross section of proton production for proton induced reactions on ^{58}Ni at (a) 100 MeV and (b) 200 MeV as a function of the laboratory angles of the outgoing protons for the energies indicated. Results of BRIC 1.4 (no evaporation) (solid histograms) and BRIC 1.0 (hashed histograms). Experimental data (stars) are from Richter *et al*. [73].

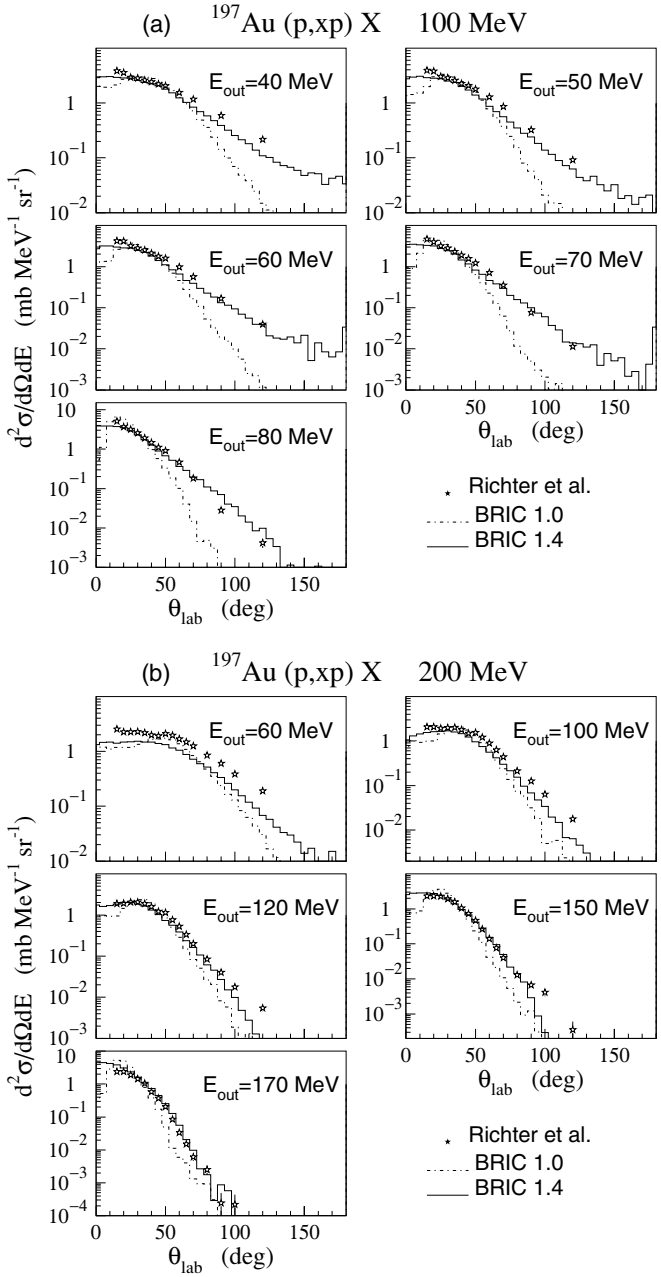

FIG. 14. Same as in Fig. 13, but for ^{197}Au.

energy. We notice that proton production decreases at very forward angles for some outgoing energies E_{out} with our older INC version (hashed histograms in Figs. 13 and 14). That decrease corresponds to the minimum of the saddle shape near 0° already seen for reactions at 62 and 65 MeV.

For proton induced reactions at 300 MeV (Fig. 15), we added the results at 10° to show the energy distribution of the outgoing protons at very forward direction in the two approaches. At this angle, the saddle shape given by BRIC 1.0 at lower incident energy is now replaced by an almost flat distribution between 50 and 250 MeV and a peak at high energy. This quasielastic peak (p, p') is broader with BRIC 1.4 as it was for (p, n) reactions [Figs. 11(b) and 12(b)], a signature of the more realistic treatment of dynamics. This change still occurs in 400 MeV proton induced reactions (Fig. 16). On the whole, the results of BRIC 1.4 are still in good agreement with proton data at these two energies. Nevertheless, emission in the backward direction is still underestimated in spite of an improvement over results with the older version.

As already mentioned, an overproduction of high energy neutrons systematically appears at forward angles between 20° and 80° for proton induced reactions between 100 and 256 MeV (Figs. 10–12). On the other hand, proton production

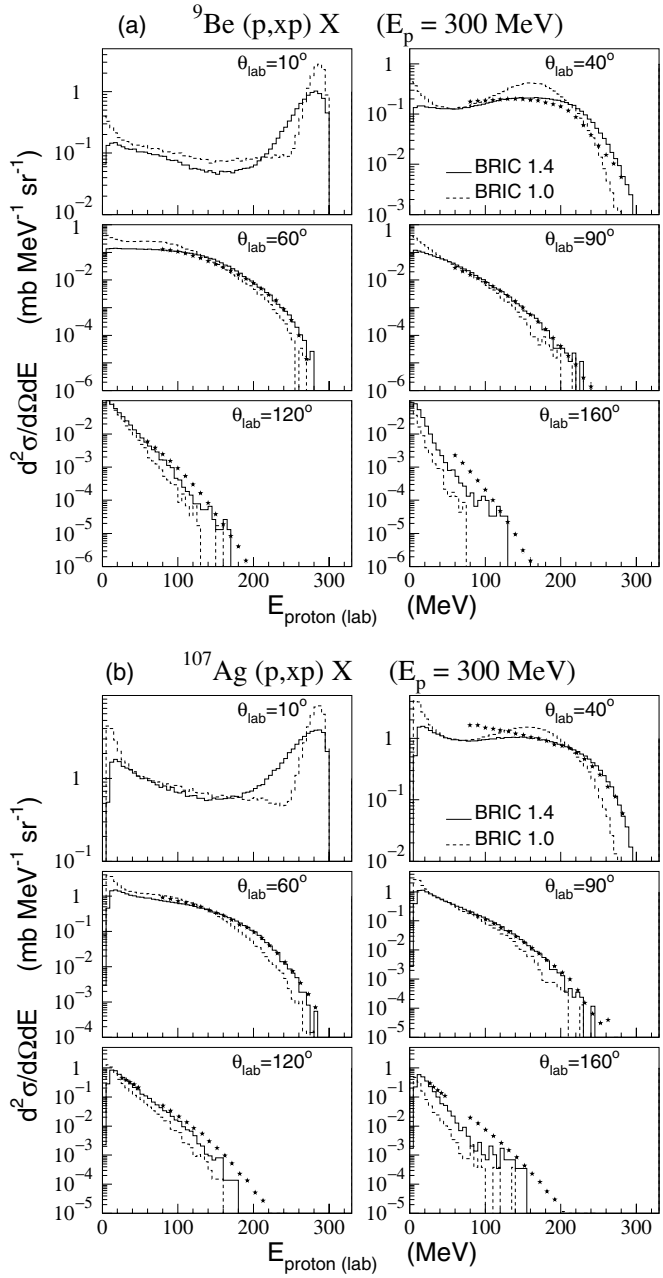

FIG. 15. Differential cross section of proton production for the reaction of 300 MeV proton on (a) ^{9}Be and (b) ^{107}Ag as a function of the energy of the proton for the angles indicated. Hashed histograms are BRIC 1.0 results; solid histograms, BRIC 1.4. Data of ^{9}Be(p, xp) and ^{107}Ag(p, xp) are from Refs. [76] and [77], respectively. No data are available at 10°.

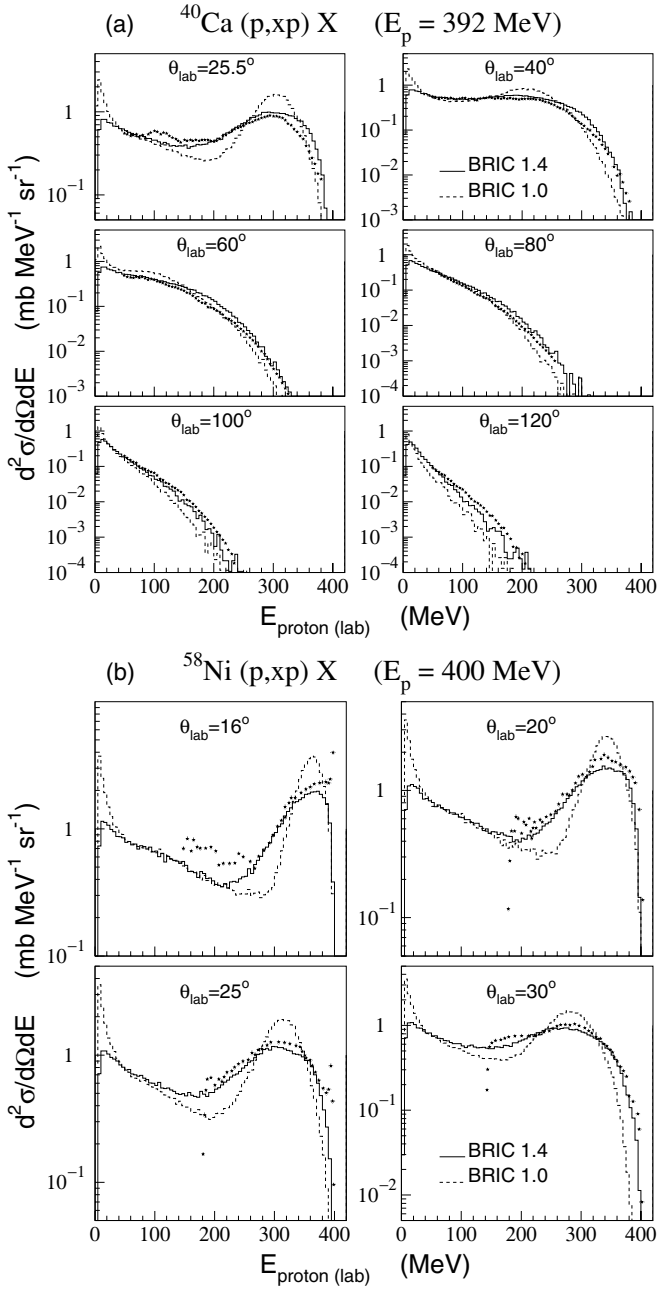

FIG. 16. Same as in Fig. 15, but for reactions (a) ^{40}Ca(p, xp) at 392 MeV with the data of Ref. [78] and (b) ^{58}Ni(p, xp) at 400 MeV with the data of Ref. [79].

in the same area of outgoing energy E_{out} and of angle θ_{lab} are in good agreement with data (see Figs. 13 and 14). This good agreement extends even up to 400 MeV for proton production in proton induced reactions (Figs. 15 and 16). There is no real inconsistency between the two results, since the potential $V_N(r)$ of neutrons is not the same as the potential $V_N(r) + V_C(r)$ of protons, and the elastic np cross sections σ_{np} and $d\sigma_{\text{np}}/d\Omega$ are also different from the pp ones. However, to correct this discrepancy, we probably will have to change the np collision term. At first glance, a change in the potential V_N does not appear to be a good solution, because the proton potential depends on it. Moreover, the difficulty of properly taking into account the $Q(p, n)$ value may contribute to this discrepancy.

Before showing high energy results, we draw some intermediate conclusions on our model for incident energies up to 400 MeV. A better treatment of the dynamics of quasifree nucleons thanks to the equations of motion and the use of the in-medium NN elastic cross sections of Li and Machleidt allow us to clearly improve the results in the very forward and backward directions. In the forward direction, above 20° (this

angle depends mostly on the incident energy), the quality of the results depends on the type of outgoing nucleon and on the incident energy: proton production is in better agreement with data than is neutron production, in this forward direction range and also for incident energies higher than 100 MeV. Our results below 100 MeV outgoing energy are of good quality except maybe in the very forward direction for INC proton emission. An underproduction of nucleons persists at the backward direction above 100 MeV incident energy. However, the shapes and yields are in better agreement with data on the whole when compared with those from our older and Bertini's INC models, with larger yields in the backward direction, a clear improvement at the very forward direction, and also improvements for lower intermediate energy reactions.

4. Reactions from 500 MeV to 1.6 GeV

We extrapolated the in-medium NN elastic cross sections of Li and Machleidt up to 500 MeV. Above this incident energy, the collision term of the incident nucleon in our present model is identical to the one calculated with the free NN cross sections (in fact, the Fermi momentum of bound nucleons makes this "transition" energy go down, but it is compensated for by the increase of the energy of the incident particle in the potential). Thus, intranuclear and outgoing nucleons above 500 MeV feel only the effect of the potential $V(r)$ through the equations of motion. The other quasifree hadrons have not only different dynamics but also different mean free paths in the two versions of BRIC.

In Fig. 17, for reactions at 597 MeV, we added the calculations at the angle 7.5° to show how the quasielastic peak (p, n) at very forward angles is changed thanks to the equations of motion. It might be surprising that this effect is rather strong at this incident energy. However, the change of momentum due to the equations of motion for protons with an impact parameter $b_{\rm inc}$ greater than $R_m(A)$ (to get mostly a peripheral collision), produces such angle deviation in the very forward direction even at intermediate energy. In that case, if we have (p, xn) or (p, xp) data at the very forward direction above ∼550 MeV, we can test the potential $V(r)$ that we have arbitrarily set.

Such data are available at 800 MeV for (p, xp) [80,81] and at 800, 1200, and 1600 MeV for (p, xn) [82]. In this paper, we present some comparisons of (p, xn) data with the potential of Eq. (6). We postpone a more complete study of the potential to a forthcoming publication. Figures 18 and 19 show some results at the three energies. Our calculations were performed with the TIERCE code to take into account the thickness of the targets (3 cm for the ^{27}Al target, for instance [82]). The quasielastic peak at 0° and 10° corresponds to neutrons between $E_{\rm inc} - 150$ MeV and $E_{\rm inc}$. In the four reactions, the maximum of the calculated peak is shifted toward a higher energy in comparison with the data. Moreover, the shapes and yields of the peak are in better agreement with our present model (solid histograms) at 800 than at 1200 MeV. At 1600 MeV, the calculated yield of the peak is higher than the data. Since the shape of the calculated peak is different from the data at 1200 MeV, we may conclude that the refraction

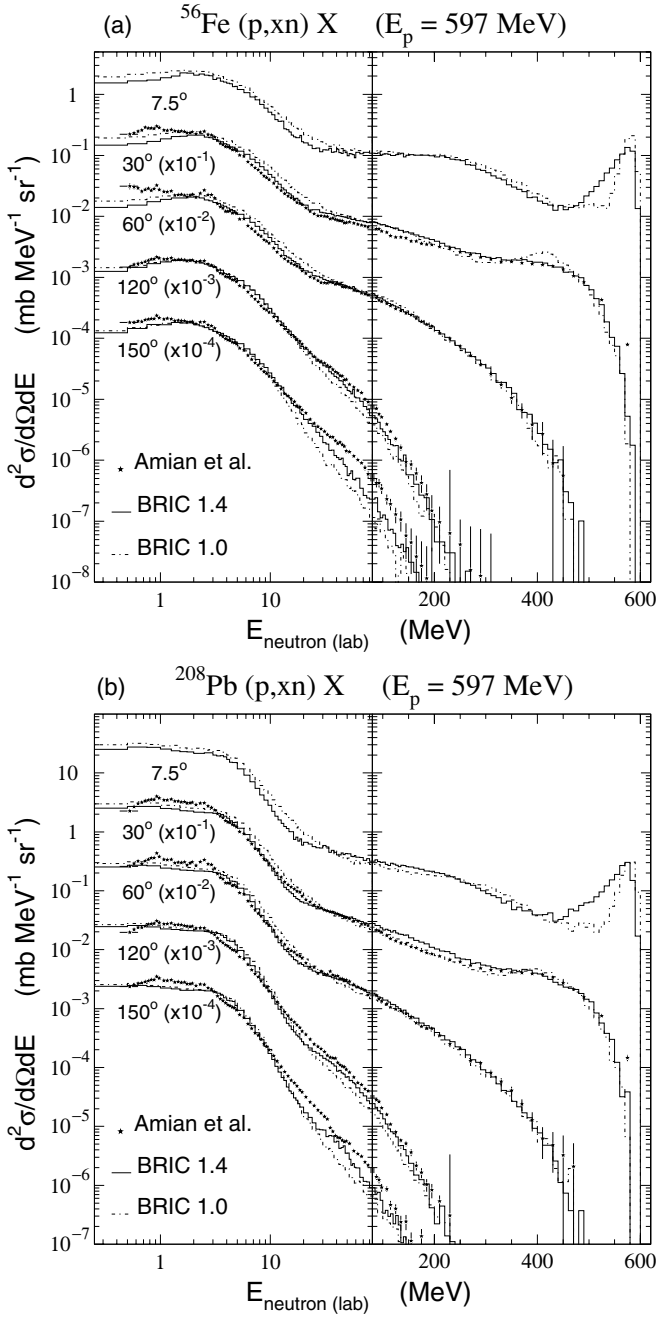

FIG. 17. Differential cross section of neutron production for reactions (a) ^{56}Fe(p, xn) and (b) ^{208}Pb(p, xn) at 597 MeV as a function of outgoing neutron energy for the angles indicated. The results of two angles are shifted by a 0.1 factor with increasing angles. The results are given in the laboratory frame. Hashed and solid histograms are the results of BRIC 1.0 and BRIC 1.4, respectively, plus evaporation. Data are from Ref. [83]. No data are available at 7.5°.

with the potential $V(r)$ of our present model is not enough to improve the results at high energy.

A broader resonance stands below the quasielastic peak at very forward angles around $E_{\rm inc} - 300$ MeV: this quasi-inelastic peak comes from the NN inelastic collision $NN \rightarrow N\Delta \rightarrow NN\pi$. The evolution of its shape and yield with the

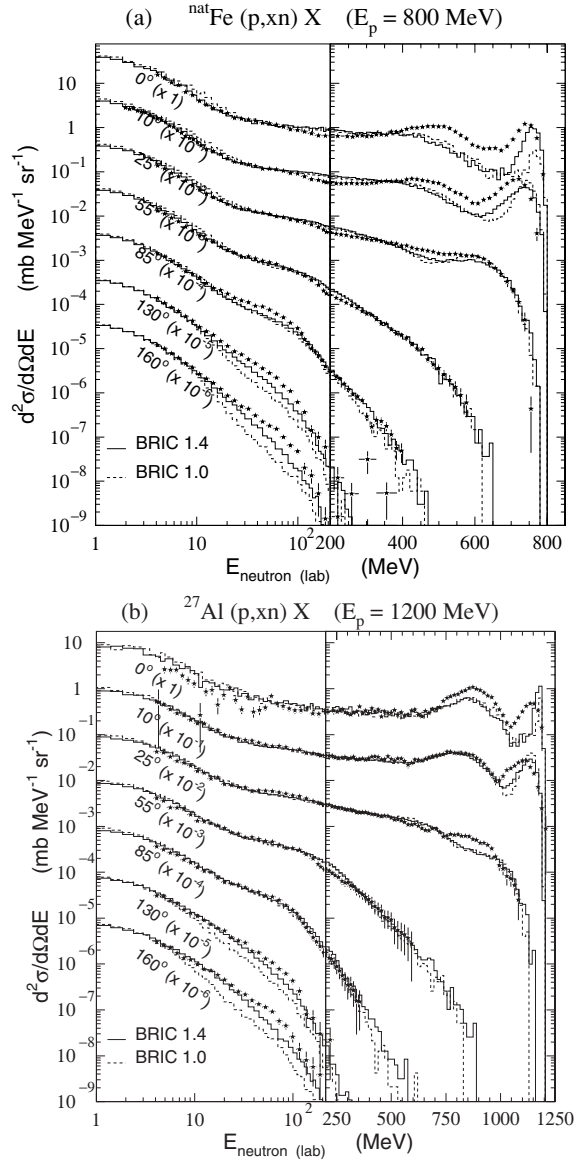

FIG. 18. Same as in Fig. 17, but for (a) 800 MeV proton on ^{nat}Fe and (b) 1200 MeV proton on ^{27}Al. Calculations were done with the TIERCE code [66] to take account of target thickness. Data are from Ref. [82].

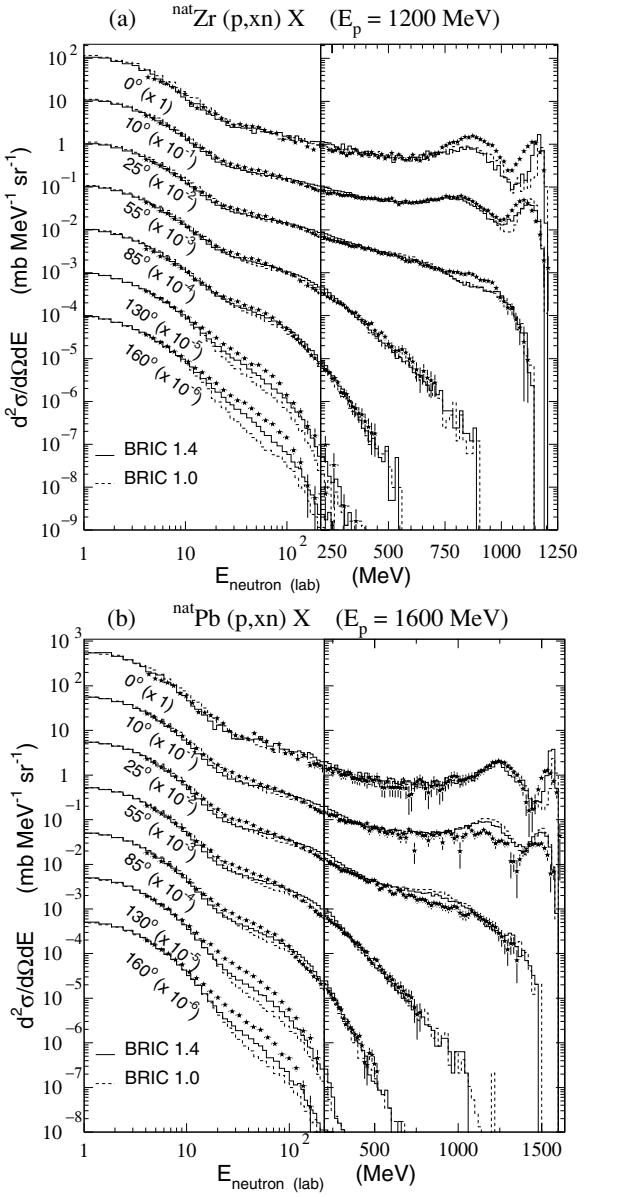

FIG. 19. Same as in Fig. 18, but for (a) 1200 MeV proton on ^{nat}Zr and (b) 1600 MeV proton on ^{nat}Pb. Calculations were done with the TIERCE code. Data are from Ref. [82].

incident energy follows more or less the data, but they still need to be improved. We notice that the refraction has no visible effect on them.

Apart from the very forward angles and the backward direction, the two versions of our INC give similar results in good agreement with data. Neutron production at intermediate angles is obviously not sensitive to refraction and to in-medium NN cross sections, which is mainly due to the high energy of the outgoing neutrons and the smooth variation of the yield with angle. In the backward direction, BRIC 1.4 predicts more intermediate energy neutrons than does BRIC 1.0, as for lower energy reactions. That compensates by a factor of 2 the large underproduction of our older version. Moreover, the evaporation area is well reproduced with our present model for reactions from 597 MeV to 1.6 GeV (Figs. 17–19).

5. *Pion production*

Figure 20 presents an example of the production of π^+ and π^- in proton induced reactions at 730 MeV and a comparison with the data of Cochran *et al*. [84]. Our INC model (BRIC 1.0 and 1.4) systematically gives an overproduction of pions in the 0–100 MeV range of outgoing energy for the reactions studied in this experiment. We observe the same trend for the reactions of 585 MeV proton on several nuclei compared with the data of Crawford *et al*. [85], even if the overproduction in the range of 0–100 MeV outgoing energy is lower than at 730 MeV (figure

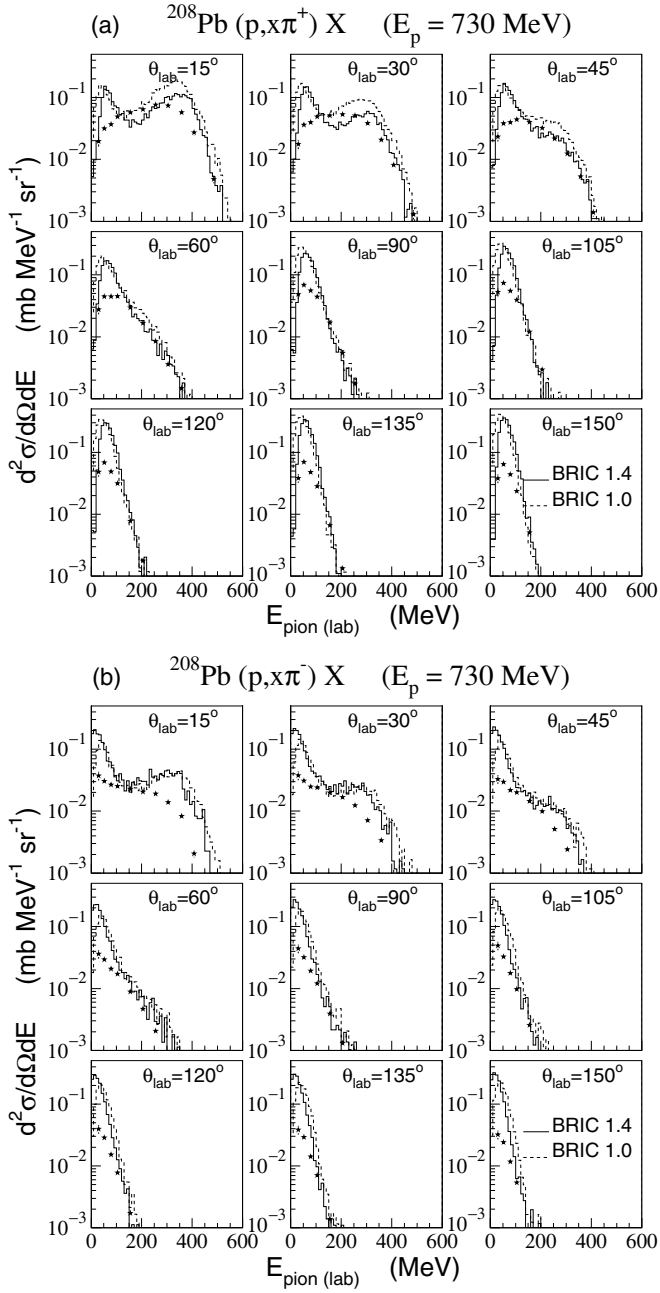

FIG. 20. Double differential cross section of outgoing (a) π^+ and (b) π^- in 730 MeV proton induced reactions on ^{208}Pb. Hashed and solid histograms are the results of BRIC 1.0 and BRIC 1.4, respectively. Symbols are data of Ref. [84].

not shown here). This discrepancy in pion emission underlines a problem in the production or the absorption of pion in the collision term. We intend to clarify this situation in the future by studying more precisely the pion induced reaction. However, this discrepancy may explain partly the difference in the mean excitation energy between BRIC and Bertini's INC at high incident energy. We recall that BRIC 1.0 and MECC-7 are based on the same approximations: no refraction, free NN cross sections, and sharp cutoff Pauli blocking. The fact that their results are similar at low intermediate energy ($\leqslant 300$ MeV) and differ at higher energy (typically >600 MeV) in terms of mean excitation energy [34] confirms our opinion that the elastic nucleon-nucleon collision terms are identical in BRIC 1.0 and in MECC-7, at least at low intermediate energy, and that the treatment of the inelastic nucleon-nucleon collision and of the pion production/absorption are different in the two INCs. Using more realistic equations of motion in BRIC 1.4 for the quasifree hadrons, including Δ's and pions, improves slightly the results in pion emission at forward angles (see solid histograms in Fig. 20) but the agreement between calculations and data is still poor. In-medium cross sections of inelastic processes could contribute to solving this problem of pion overproduction, but we expect more from the $\pi d \rightleftharpoons NN$ process, which is not yet explicitly included in our approach.

6. *Higher t_{cut} for low energy neutron reactions?*

To end our systematic comparison of particle production in nucleon induced reactions, we present the full calculation of the neutron induced reaction below 20 MeV with BRIC 1.4 and evaporation/fission. Figures 21(a) and 22(a) present the results with $t_{cut} = 100$ fm/c for two reactions, 18 MeV neutrons on ^{238}U and 14 MeV neutrons on ^{209}Bi, respectively. The solid histograms are the sum of the INC and the deexcitation stages, the fill areas show the INC component. In the latter, the elastic peak and contributions from discrete levels are of course missing. However, we obtained an estimation of the contribution of the continuum with our model that is not so different from the data in the forward direction. We notice a slow decrease of the yield of this INC component with angle in the forward direction which continues toward backward angles. For the reaction of neutron on ^{209}Bi (Fig. 22), data cover angles up to 150°. Since fission of bismuth is not significant at this incident energy, neutrons from fission products are absent, which allows a straight comparison of preequilibrium emissions. At the backward angles, the yields of neutrons with energy higher than 7 MeV (above the evaporation component) from the INC component are much smaller than the data.

Since the incident nucleon has a low energy, we may expect that the nonelastic reaction takes a longer time because of the refraction, this is even truer for heavy nuclei. We then apply a higher time cut. $t_{cut} = 200$ fm/c allows us to get most of the outgoing neutrons by decreasing the probability of having quasifree nucleons inside the nucleus at t_{cut}.

Figures 21(b) and 22(b) present the same results as before with $t_{cut} = 200$ fm/c for the two reactions. We now get larger productions of neutrons in the backward direction that are in better agreement with data. For the two reactions, the yields of neutrons from our INC model are more than one order of magnitude larger with the new t_{cut} at 160° or more. The double differential of neutron production at four outgoing energies are detailed at four times in Fig. 23 for the 14 MeV neutron on ^{209}Bi. While emission in the forward direction occurs essentially before 100 fm/c, the backward emission still continues after 125 fm/c. The difference of neutron yields is very slight between 150 and 200 fm/c for the highest outgoing energies ($E_{out} \geqslant 8$ MeV); however, as it can be seen for low outgoing energies, the difference in yields is always at backward angles.

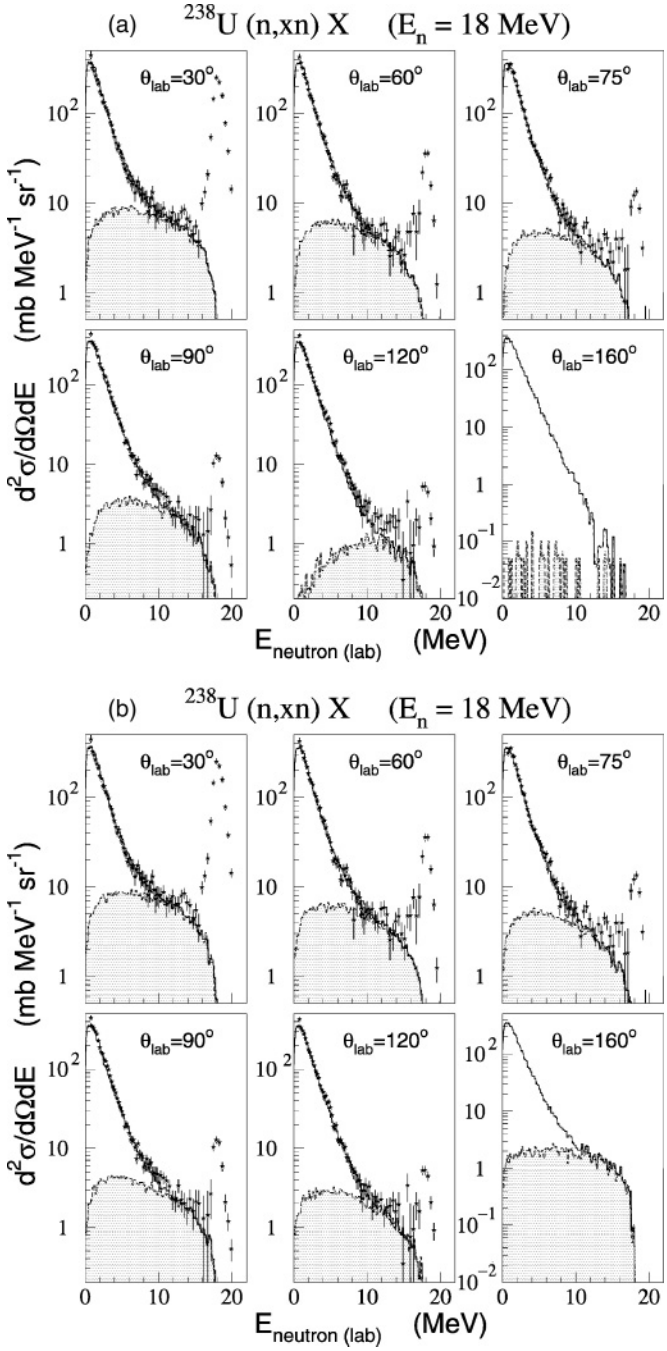

FIG. 21. Double differential cross section of neutron production in 18 MeV neutron induced reaction on ^{238}U with BRIC 1.4 for two cuts of the time of reaction: (a) 100 fm/c and (b) 200 fm/c. Data are from Ref. [86]. No data are available at 160°. Filled area is the INC component; solid histograms, sum of INC and deexcitation components (including evaporation of fission fragments).

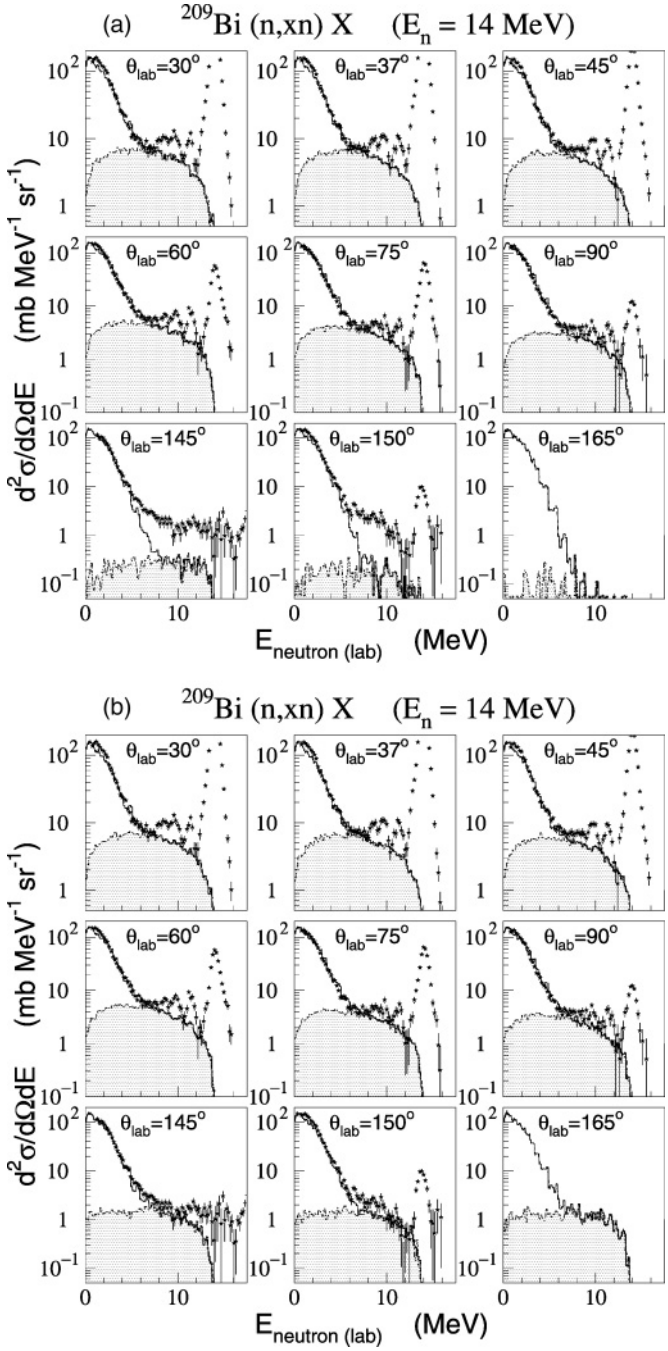

FIG. 22. Same as in Fig. 21, but for 14 MeV neutrons on ^{209}Bi. Data are from Ref. [87]. No data available at 165°.

Figure 24 shows some typical trajectories of quasifree neutrons emitted in the backward direction in nonelastic reactions induced by 14 MeV neutrons on ^{209}Bi. In these examples, trajectories are projected on the $[\pm(x^2 + y^2)^{1/2}, z]$ plane, and nonelastic events finish at t_{out}, the time of emission of the quasifree neutron. Example (b) includes a reflexion of the outgoing neutron on the nucleus edge (dotted-line circle) followed by its backward emission. Two effective collisions occur in example (c), the quasifree neutron goes backward in the second $n_{qf}N_{bound}$ collision. In examples (a) and (d), quasifree neutrons have a kinetic energy around $E_{out} + e_{bind}$ between t_{coll} and t_{out}, the corresponding distances are then lower than the trajectories before t_{coll} when they get more kinetic energy thanks to the potential V. We can conclude that a time cut of 100 fm/c ends prematurely some of the nonelastic events, more specifically, events where quasifree neutrons (before or after a nn or np collision) are still moving in the nuclear volume but have not yet reached its edge. A too short

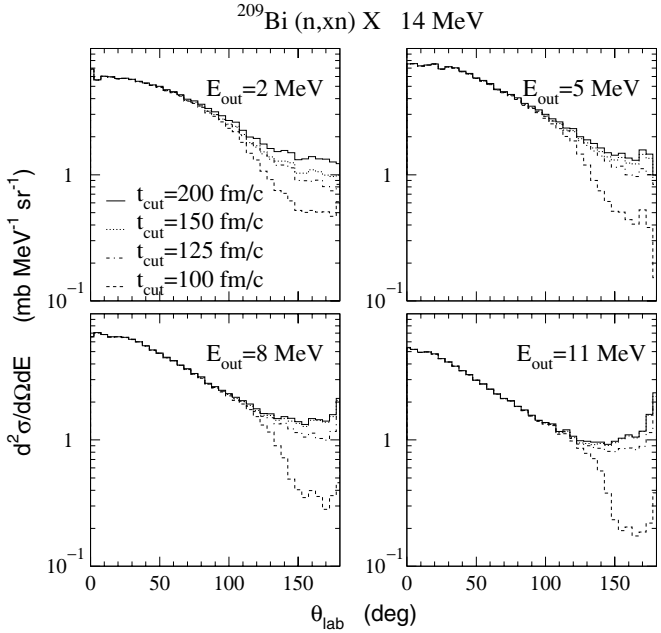

FIG. 23. Double differential cross section of neutron production for four outgoing energies in the 14 MeV neutron induced reaction on ^{209}Bi. Results of BRIC 1.4 are shown at four $t_{\rm cut}$ levels as indicated in legend.

$t_{\rm cut}$ cuts the backward emission more strongly than the forward emission. That comes from the longer trajectories of quasifree neutrons emitted in the backward direction due to refraction or reflexion. Higher values of $t_{\rm cut}$ produce statistically the same results with our present definition of $R_{\rm limit}$, thus we can set $t_{\rm cut} \sim 200$ fm/c in BRIC 1.4 to complete the full INC stage at low incident energy (10–30 MeV).

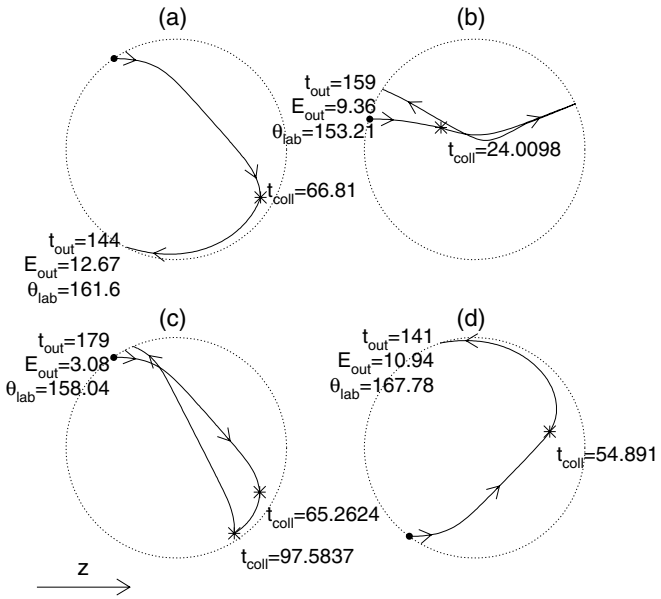

FIG. 24. Some trajectories of backward emitted neutrons in 14 MeV neutron induced reaction on ^{209}Bi. Positions of incident neutron at $t = 0$ (black dots) and of effective collision at time $t_{\rm coll}$ (black crosses) are given in $[\pm(x^2 + y^2)^{1/2}, z]$ plane and in nucleus rest frame. Dotted line circle is the nucleus edge ($R_{\rm limit} = 9.58$ fm). Momentum of incident neutron is along z axis with $p_z > 0$, and arrows indicate direction. $E_{\rm out}$, $\theta_{\rm lab}$, and $t_{\rm out}$ are the kinetic energy of emitted neutron (MeV), angle of emission (deg), and time of emission (fm/c), respectively.

In the study of the neutron multiplicity in fission of ^{238}U and ^{235}U with neutrons up to 200 MeV [37], the time cut used in the calculation was 100 fm/c. We recall that cuts on energy were applied in the evaporation area ($0.8 < E_{\rm out} < 7.5$ MeV) to compare with experimental data. In this energy region, the INC component is small in comparison with the evaporation component. Then the underestimation of neutron multiplicity is small in the 20–30 MeV BRIC 1.4 calculations in this paper.

IV. CONCLUSION

Calculations of particle production were performed for 125 nucleon induced reactions with available experimental data, some results were presented here. Among those reactions, 112 were performed with incident energies of less than 600 MeV. The incident energies range from 14 to 1600 MeV and target nuclei range from Be to U. This systematic study allows us to confirm that a more realistic treatment is needed of the dynamics of the quasifree hadrons and the in-medium NN elastic cross sections because they play a significant role in the energy-angular distributions of emitted nucleons during the INC stage.

After the analysis of low intermediate energy reactions, we may conclude that the flat distribution of outgoing energy at forward angles in (p, xp) and (p, xn) reactions comes mainly from refraction in our present model. The in-medium NN elastic cross sections of Li and Machleidt improve the results even more, especially by increasing the mean free path and then by decreasing the yield of low energy nucleons. Thus, compared to our older INC model and Bertini's INC model, the present model usually corrects the saddle shape present in the very forward direction and the systematic underproduction in the backward direction at low intermediate energy (40–100 MeV). At intermediate energy (100–600 MeV), our results are of rather good quality. We notice an overproduction of the higher energy neutrons in the forward direction above 20° in 100–250 MeV proton induced reactions. A better agreement with data is obtained for (p, xp) reactions than for (p, xn). We expect the same conclusion for (n, xn) reactions in comparison to (n, xp). An underproduction of nucleons in the backward direction starts to be visible and increases with the incident energy. At higher incident energies (600–1600 MeV), our results are in good agreement except in the quasielastic and quasi-inelastic peaks and in the backward direction. Results in the backward direction are nevertheless better with our present model than with our older one thanks to the combined effects of the refraction and the in-medium NN cross sections. The pions are also overproduced in this energy range.

We may state that our current results are on the whole in good agreement with data, both for the INC component and for the sum of INC and evaporation, for a large range of incident energies and target nuclei. The phase space dynamics of the quasifree hadrons only and a potential which is not self-consistent constitute the main differences between our

approach and some sophisticated models (BUU-like models). A self-consistent potential should not be essential in nucleon induced reactions, and the dynamics of most of the bound nucleons might also not be useful. Moreover, these approximations allow us to reduce computing times: for one full event (INC and deexcitation), BRIC 1.0 is less than 2 times slower than MECC-7 and BRIC 1.4 is around 4 times slower than BRIC 1.0 whatever the incident energy and the target nuclei. Thus we reach a good compromise between the quality of results and computing time.

At low intermediate energy, our present INC model gives results similar to most preequilibrium models. This should not be surprising: by definition the INC model shares the same basic physics than the semiclassical preequilibrium. What is more surprising is that INC uses the impulse approximation. However, we merely observe that the combined effects of the in-medium NN cross sections and the dynamics of quasifree nucleons, on one hand, and of the rather simple Pauli blocking (sharp cutoff), collision term (deduced from distance of minimal approach) without N-body collisions, and description of the nucleus, on the other hand, produce results of "preequilibrated" nucleon emission of good quality on average. Thus, most of the physics is probably included in our approach for the emission of nucleons even though small systematic discrepancies remain.

Is an equilibration step needed to go from the INC stage to statistical evaporation of the compound nucleus? The work done with the QMD model [31–33] shows that sophisticated nuclear dynamics models may simulate the fast step and some classical equilibration of the nonelastic reaction. The comparison of QMD results with those of the Feshbach-Kerman-Koonin (FKK) preequilibrium model tends to confirm this conclusion [33,88]. From the comparisons of our calculations with data, we can reach the same conclusion. However, it is interesting to note that equilibration is not treated as fully in our present model as it is in the QMD model, since our model allows no collision between bound nucleons. By doing so, the emission of low energy nucleons is certainly damped before t_{cut}, but we expect, first, that this emission of low energy nucleons in the INC stage would be small due to the refraction of their trajectory and their reflexion on the potential well, and secondly, that this emission would be similar to the evaporation process. The fact that the emission of low energy nucleons coming from a *bound bound* $\rightarrow$ *bound quasifree* collision is suppressed in the INC stage is certainly not crucial if we look at the final results of the full reaction INC+deexcitation. In some way, the low energy nucleons that are not emitted in the INC stage will be emitted in the deexcitation stage. What is more important is the emission of preequilibrated particles. Regarding that point, we notice an influence of the t_{cut} parameter on the preequilibrated neutron emission; however it is more crucial at small incident energy, around 10–30 MeV. This observation leads us to the conclusion that the influence of the dynamics on equilibration is far from being negligible.

The underproduction of nucleons at the backward direction is a systematic discrepancy in our calculations which increases with the incident energy. Although other mechanisms can contribute to improving that discrepancy, we expect that the scattering on clusters inside the nucleus is necessary, as Blann and collaborators [15] have already concluded. This process is indeed another cause of particle production at backward angles [89,90]. A study of the sensitivity on the potential parametrization is necessary to settle the results of the present classical approach. Improvement of the pion production should be easier if we focus our attention on pion induced reaction. It will also certainly need quasideuteron absorption. The influence of in-medium cross sections on the quasielastic and quasi-inelastic peaks has already been studied for 1200 MeV proton induced reactions with the UrQMD model [91]. Such in-medium cross sections should also influence pion production. But first of all, we plan to include the emission of light charged composites in the near future, since it is the most missing process in our current model. Although the coalescence model [92] has been successfully applied by Mashnik *et al.* in the Cascade Exciton Model [93], and by Cugnon *et al.* in the INC of Liège (INCL) model [94] with a recent update [95], we intend to try another approach.

To summarize our work, we have assumed that an INC approach with improvements inspired from sophisticated dynamic nuclear models can be enough to describe the first part of nonelastic reactions induced by nucleons without the help of an additional preequilibrium model before the deexcitation stage. Our current INC model gives good results on average for a large range of incident energies and target nuclei even at low intermediate energy well below the accepted limit of the impulse approximation. Thus no preequilibrium model is necessary between our current intranuclear cascade BRIC 1.4 and the deexcitation stage since it effectively includes the preequilibrium emission.

ACKNOWLEDGMENTS

The author would like to thank O. Bersillon for his support and encouragement on this work. Thanks are also due to E. Bauge for a careful reading of the manuscript and helpful comments and to J. L. Sida for pertinent suggestions. The author is also grateful to B. Morillon and P. Romain for useful discussion and optical model calculations.

[1] R. Serber, Phys. Rev. **72**, 1008 (1947).
[2] H. Bertini, Phys. Rev. **131**, 1801 (1963); **138**, AB2 (1965).
[3] H. W. Bertini, Phys. Rev. **188**, 1711 (1969); Phys. Rev. C **6**, 631 (1972).
[4] K. Chen *et al.*, Phys. Rev. **166**, 949 (1968).
[5] V. S. Barashenkov, K. K. Gudima, and V. D. Toneev, Acta Phys. Pol. **36**, 415 (1969).
[6] V. S. Barashenkov, B. F. Kostenko, and A. M. Zadorogny, Nucl. Phys. **A338**, 413 (1980).
[7] J. D. Stevenson, Phys. Rev. Lett. **41**, 1702 (1978).
[8] Y. Yariv and Z. Fraenkel, Phys. Rev. C **20**, 2227 (1979).

[9] J. Cugnon, Phys. Rev. C **22**, 1885 (1980).
[10] J. Cugnon, Nucl. Phys. **A462**, 751 (1987).
[11] A. Boudard, J. Cugnon, S. Leray, and C. Volant, Phys. Rev. C **66**, 044615 (2002).
[12] J. J. Griffin, Phys. Rev. Lett. **17**, 478 (1966).
[13] G. D. Harp, J. M. Miller, and B. J. Berne, Phys. Rev. **165**, 1166 (1968).
[14] M. Blann, Annu. Rev. Nucl. Sci. **25**, 123 (1975).
[15] M. Blann, W. Scobel, and E. Plechaty, Phys. Rev. C **30**, 1493 (1976).
[16] K. K. Gudima, S. G. Mashnik, and V. D. Toneev, Nucl. Phys. **A401**, 329 (1983).
[17] F. E. Bertrand and R. Peele, Phys. Rev. C **8**, 1045 (1973).
[18] H. W. Bertini, G. D. Harp, and F. E. Bertrand, Phys. Rev. C **10**, 2472 (1974).
[19] A. Galonsky *et al*., Phys. Rev. C **14**, 748 (1976).
[20] M. M. Meier *et al*., Nucl. Sci. Eng. **102**, 102 (1989).
[21] M. M. Meier *et al*., Nucl. Sci. Eng. **110**, 289 (1992).
[22] T. W. Armstrong and K. C. Chandler, Nucl. Sci. Eng. **49**, 110 (1972).
[23] R. E. Prael and H. Lichtenstein, User Guide to LCS: The LAHET Code System," Los Alamos National Laboratory Report No. LA-UR-89-3014, 1989.
[24] L. S. Waters ed., MCNPX User's Manual, Version 2.3.0, Los Alamos National Laboratory report LA-UR-02-2607, April 2002.
[25] J. Briesmeister ed., "MCNP - A General Monte Carlo *N*-Particle Transport Code, Version 4C" Los-Alamos, LA-13709-M, April 2000.
[26] M. B. Chadwick *et al*., Nucl. Sci. Eng. **131**, 293 (1999).
[27] G. F. Bertsch and S. Das Gupta, Phys. Rep. **160**, 189 (1988).
[28] A. Bonasera, F. Gulminelli, and J. Molitoris, Phys. Rep. **243**, 1 (1994).
[29] J. Aichelin, Phys. Rep. **202**, 233 (1991).
[30] H. Stöcker and W. Greiner, Phys. Rep. **137**, 277 (1986).
[31] G. Peilert, J. Konopka, H. Stocker, W. Greiner, M. Blann, and M. G. Mustafa, Phys. Rev. C **46**, 1457 (1992).
[32] K. Niita, S. Chiba, T. Maruyama, T. Maruyama, H. Takada, T. Fukahori, Y. Nakahara, and A. Iwamoto, Phys. Rev. C **52**, 2620 (1995).
[33] S. Chiba, M. B. Chadwick, K. Niita, T. Maruyama, T. Maruyama, and A. Iwamoto, Phys. Rev. C **53**, 1824 (1996).
[34] H. Duarte, in *Proceedings of the Third International Conference on Accelerator-Driven Transmutation Technologies and Applications*, Praha, Czech Republic, June 7–11, 1999.
[35] F. Wrobel, J. M. Palau, M. C. Calvet, O. Bersillon, and H. Duarte, IEEE Trans. Nucl. Sci. **47**, 2580 (2000).
[36] D. Lambert *et al*., IEEE Trans. Nucl. Sci. **52**, 2332 (2005).
[37] T. Ethvignot, M. Devlin, H. Duarte, T. Granier, R. C. Haight, B. Morillon, R. O. Nelson, J. M. ODonnell, and D. Rochman, Phys. Rev. Lett. **94**, 052701 (2005).
[38] J. F. Clerjeau, L. Roux, J. P. Delaroche, and O. Bersillon, (private communication).
[39] J. F. Berger, M. Girod, and D. Gogny, Comput. Phys. Commun. **63**, 365 (1990), and references therein.
[40] Y. Kitazoe, M. Sano, Y. Yamamura, H. Furutani, and K. Yamamoto, Phys. Rev. C **29**, 828 (1984).
[41] C. Y. Wong, Phys. Rev. C **25**, 1460 (1982).
[42] G. F. Bertsch, H. Kruse, and S. Das Gupta, Phys. Rev. C **29**, 673 (1984).
[43] A. Messiah, *Quantum Mechanics* (North-Holland, Amsterdam, 1958), Vol. 1.
[44] P. Fröbrich, R. Lipperheide, and K. Möhring, Z. Phys. B **78**, 325 (1990).
[45] Gy. Wolf *et al*., Nucl. Phys. **A517**, 615 (1990).
[46] J. Cugnon, C. Vollant, and S. Vuillier, Nucl. Phys. **A620**, 475 (1997).
[47] T. Kodama, S. B. Duarte, K. C. Chung, R. Donangelo, and R. A. M. S. Nazareth, Phys. Rev. C **29**, 2146 (1984).
[48] G. Q. Li and R. Machleidt, Phys. Rev. C **48**, 1702 (1993); **49**, 566 (1994).
[49] T. Alm, G. Röpke, and M. Schmidt, Phys. Rev. C **50**, 31 (1994).
[50] E. Suetomi, N. Kishida, and H. Kadotani, Phys. Lett. **B333**, 22 (1994).
[51] B. J. VerWest and R. A. Arndt, Phys. Rev. C **25**, 1979 (1982).
[52] J. H. Koch, E. J. Moniz, and N. Ohtsuka, Ann. Phys. (NY) **154**, 99 (1984).
[53] J. Cugnon, S. Leray, E. Martinez, Y. Patin, and S. Vuillier, Phys. Rev. C **56**, 2431 (1997).
[54] T. Rupp *et al*., Phys. Rev. C **28**, 1696 (1983).
[55] J. Cugnon, T. Mizutani, and J. Vandermeulen, Nucl. Phys. **A352**, 505 (1981); J. Cugnon and R. M. Lombard, *ibid.* **A422**, 635 (1984).
[56] M. Blann, H. Gruppelaar, P. Nagel, and J. Rodens, *International Code Comparison for Intermediate Energy Nuclear Data* (OECD/NEA, Paris, France, 1994).
[57] J. Cugnon and P. Henrotte, Eur. Phys. J. A **16**, 393 (2003).
[58] S. Chiba, K. Niita, and O. Iwamoto, Phys. Rev. C **54**, 3302 (1996).
[59] J. Franz *et al*., Nucl. Phys. **A510**, 774 (1990).
[60] P. A. Piroue and J. S. Smith, Phys. Rev. **148**, 1315 (1966).
[61] V. F. Weisskopf and D. H. Ewing, Phys. Rev. **57**, 472 (1940).
[62] A. V. Ignatyuk, G. N. Smirenkin, and A. S. Tishin, Sov. J. Nucl. Phys. **21**, 255 (1975).
[63] F. Atchison, in *Proceedings of a Specialists' Meeting* (OECD/NEA, Issy-le-Moulineaux, France, 1994), p. 199.
[64] J. V. Lepore and R. N. Stuart, Phys. Rev. **94**, 1724 (1954).
[65] E. Gradsztajn, Ann. Phys. (Paris) **10**, 791 (1965); E. Gradsztajn *et al*., Phys. Rev. Lett. **14**, 436 (1965).
[66] O. Bersillon, in *Proceedings of the Second International Conference on Accelerator-Driven Transmutation Technologies and Applications*, Kelmar, Sweden, 3–7 June 1996, edited by H. Conde, Vol. I-II (Uppasala University, Department of Neutron Research, 1997), p. 520.
[67] A. J. Koning and J. P. Delaroche, Nucl. Phys. **A713**, 231 (2003).
[68] H. Sakai *et al*., Nucl. Phys. **A344**, 41 (1980).
[69] M. Blann *et al*., Nucl. Phys. **A257**, 15 (1976).
[70] M. Trabandt, W. Scobel, M. Blann, B. A. Pohl, R. C. Byrd, C. C. Foster, and R. Bonetti, Phys. Rev. C **39**, 452 (1989).
[71] A. A. Cowley *et al*., Phys. Rev. C **43**, 678 (1991).
[72] W. Scobel, M. Trabandt, M. Blann, B. A. Pohl, B. A. Remington, R. C. Byrd, C. C. Foster, R. Bonetti, C. Chiesa, and S. M. Grimes, Phys. Rev. C **41**, 2010 (1990).
[73] W. A. Richter, A. A. Cowley, R. Lindsay, J. J. Lawrie, S. V. Fortsch, J. V. Pilcher, R. Bonetti, and P. E. Hodgson, Phys. Rev. C **46**, 1030 (1992).
[74] W. A. Richter *et al*., Phys. Rev. C **49**, 1001 (1994).
[75] W. A. Richter *et al*., Phys. Rev. C **54**, 1756 (1996).
[76] R. E. L. Green *et al*., Nucl. Phys. **A405**, 463 (1983).

[77] R. E. L. Green, R. G. Korteling, J. M. D'Auria, K. P. Jackson, and R. L. Helmer, Phys. Rev. C **35**, 1341 (1987).
[78] A. A. Cowley, G. F. Steyn, Y. Watanabe, T. Noro, K. Tamura, M. Kawabata, K. Hatanaka, H. Sakaguchi, H. Takeda, and M. Itoh, Phys. Rev. C **62**, 064604 (2000).
[79] H. Esbensen and G. F. Bertsch, Phys. Rev. C **34**, 1419 (1986).
[80] R. E. Chrien, T. J. Krieger, R. J. Sutter, M. May, H. Palevsky, R. L. Stearns, T. Kozlowski, and T. Bauer, Phys. Rev. C **21**, 1014 (1980).
[81] J. A. McGill, G. W. Hoffmann, M. L. Barlett, R. W. Fergerson, E. C. Milner, R. E. Chrien, R. J. Sutter, T. Kozlowski, and R. L. Stearns, Phys. Rev. C **29**, 204 (1984).
[82] X. Ledoux *et al*., Phys. Rev. Lett. **82**, 4412 (1999); S. Leray *et al*., Phys. Rev. C **65**, 044621 (2002).
[83] W. B. Amian *et al*., Nucl. Sci. Eng. **115**, 1 (1993).
[84] D. R. F. Cochran *et al*., Phys. Rev. D **6**, 3085 (1972).
[85] J. F. Crawford *et al*., Phys. Rev. C **22**, 1184 (1980).
[86] M. Baba, H. Wakabayashi, N. Ito, K. Maeda, and N. Hirakawa, J. Nucl. Sci. Technol. **27**, 601 (1990).
[87] M. Baba, S. Matsuyama, T. Ito, T. Ohkubo, and N. Hirakawa, J. Nucl. Sci. Technol. **31**, 757 (1994).
[88] M. B. Chadwick, S. Chiba, K. Niita, T. Maruyama, and A. Iwamoto, Phys. Rev. C **52**, 2800 (1995).
[89] T. Fujita, Phys. Rev. Lett. **39**, 174 (1977).
[90] P. Danielewicz, Phys. Rev. C **42**, 1564 (1990).
[91] K. Abdel-Waged, Phys. Rev. C **70**, 014605 (2004).
[92] D. H. Boal, Phys. Rev. C **25**, 3068 (1982).
[93] S. G. Mashnik, Nucl. Phys. **A568**, 703 (1994).
[94] J. Cugnon and C. Volant, Z. Phys. A **334**, 435 (1989).
[95] A. Boudard *et al*., Nucl. Phys. **A740**, 195 (2004).